The complex nonstoichiometry of wüstite Fe 1- O: review and comments

Jean-Raymond Gavarri, Claude Carel

▶ **To cite this version:**

The complex nonstoichiometry of wüstite Fe$_{1-z}$O: review and comments

Jean-Raymond Gavarri [1*] and Claude Carel [2]

[1] *University of Toulon, Aix Marseille Univ., CNRS 7334, IM2NP, Toulon, France.*
  BP 20132, 83957 La Garde Cedex, France
* *to whom correspondence must be addressed* - e-mail = gavarri.jr@univ-tln.fr

[2] *Honorary Professor, University of Rennes1, 2 rue du Thabor CS 46510, 35065 Rennes Cedex, France*
  e-mail = c-carel@orange.fr

Abstract

Thermodynamic properties and structural aspects of the nonstoichiometric wüstite Fe$_{1-z}$O, and its modifications - the so-called pseudo-phases - as functions of departure z from stoichiometry and of equilibrium temperature are reviewed from 1960 to present. The complexity of the equilibrium phase diagram is described in some details. The first order transition W $\leftrightarrows$ W' is specified on the iron/wüstite boundary near 1185 K. Transitions correlated to the modifications Wi at T(W)>1185 K and W'j at T(W') <1185 K (i and j =1,2,3) are re-examined. Structural determinations based on the characterization of point defects stabilization and of their clustering are reviewed. Additionally, the pseudo-phases are examined based on the transformation of defect clusters or of their mode of distribution (*i.e.,* percolation or superstructure) with the inclusion of changes in electronic charge carriers.

Keywords: **wüstite, alpha-gamma transition, point defects, defect clusters, pseudo-phases, percolation**

1. Introduction

The nonstoichiometric iron monoxide Fe$_{1-z}$O is the main constituent of traditional blast furnace slags. Historically, this oxide was the subject of numerous studies in the general context of iron metallurgy improvement, and for its role in the fields of recycling of industrial waste, catalysis and nanoparticles. Fe$_{1-z}$O, also written equivalently as Fe$_y$O or FeO$_x$, is named after the German mineralogical appellation "wüstit"[1]. The wüstite is considered of particular interest by the geophysicists because it is a constituent of the lower mantel of earth. This oxide is in a steady state, between an invariant point near 600 °C and its melting temperature around 1400 °C, under an equilibrium oxygen pressure p' in the range 10^{-25} to 10^{-6} bar. Its large iron deficiency is expressed by the departure of stoichiometry $z \in$ [0.04 - 0.18] around 1400 °C and $z \cong 0.065$ near 600 °C.

Because of so many papers published before, numerous reviews about the nonstoichiometric wüstite are available in the literature. So, the present authors make choices of some of them or equivalent works:

Goodenough [1], Kofstad [2], Vallet [3], Burgmann [4], Gokcen [5], Men' *et al.* [6], Spencer, Kubaschewski [7], Bauer, Pianelli [8], Sorensen [9], Hazen, Jeanloz [10], Gleitzer, Goodenough[11], Gokcen [12], Lykasov *et al.* [13], Mrowec, Podgorecka [14], Long, Grandjean [15], Sundman [16], Wriedt [17], Collongues [18], Gleitzer [19], Smyth [20], Desré, Hodaj [21], Worral, Coley [22].

---

[1] There is no equivalent available in the English language for the German phoneme 'ü'.

Multiple studies have addressed the nature of the point defects (iron vacancies and interstitials) in wüstite, and the concept of defect clustering was systematically developed with a large variety of structural models. The NaCl face centered cubic structure of wüstite is characterized by a high rate of iron vacancies, and the existence of a certain proportion of iron ions occupying interstitial sites. Crystallographic determinations showed that these defects are not disordered in the lattice. Diverse models of clusters of iron vacancies and interstitials have been proposed.

Because it simplifies the structural description of defects, the oxygen site is assumed to be fully occupied (*i.e.*, there is no significant amount of oxygen vacancies). Adopting the notation of Kröger and Vink [23], the formula of this monoxide can be developed as

$$\textbf{Fe}_{1-z}\textbf{O} = (\textbf{Fe}_{\textbf{Fe}})_{(1-3z)}(\textbf{Fe}_{\textbf{Fe}}^{\circ})_{(2z-t)}(\textbf{Fe}_{\textbf{i}}^{\circ\circ\circ})_{t}(\textbf{V}_{\textbf{Fe}}^{\textbf{q}(\prime)})_{(z+t)}\textbf{O}_{\textbf{O}} \qquad (1)$$

The ionic species Fe^{2+} and Fe^{3+}, in octahedral sites, are noted Fe_{Fe} and Fe_{Fe}°. The Fe^{3+} cations in tetrahedral (interstitial) sites are noted $Fe_{i}^{\circ\circ\circ}$. Iron vacancies noted $V_{Fe}^{q(\prime)}$ can be charged negatively corresponding to q=2 or q=1, or neutral corresponding to q=0. Electric neutrality would result from electrons jumping in the conduction band or interacting with holes in the valence band. It can be recalled that the band gap of wüstite was recently evaluated at about 1.0 eV at 25 °C, which means that a large population of electrons in the conduction band and/or holes in the valence band can be expected at high temperature, depending on the oxygen partial pressure [24].

In this paper, we review historical (1960-2014) observations and concepts for wüstite at equilibrium and in quenched samples. Then, we show how the complex nonstoichiometry of wüstite can be better described using mixtures of point defects and their associations in clusters which fall into order progressively at increasing *z*.

2. The complex behavior of wüstite

2.1. Early work (1921-1961)

In 1921, **G. Chaudron** worked in H. Le Chatelier's lab. when he determined experimentally the external boundaries of the stable domain of ferrous oxide considered to be the daltonide 'FeO' [25]. Point C is at the intersection of the two boundaries, where three solid phases (Fe, Fe3O4 and 'FeO') coexist at equilibrium at 570°C, temperature that has been revised particularly by Raccah, Vallet, Carel [26-29], and that is named Chaudron's point.

Jette and Foote demonstrated -measurements of the cell parameter and density- that wüstite was an iron deficient solid solution. They deducted that for the ionic compound, a missing Fe^{2+} was necessarily compensated by the oxidation of two other Fe^{2+} giving rise to electron holes Fe^{3+} [30].

Darken and Gurry studied in detail the phase diagram when determining the composition of wüstite chemically after slow quenching from Θ °C= 1100, 1200, 1300 and 1400. The boundaries with iron and magnetite were determined down to Chaudron's point. Additionally, the authors determined exhaustively the molar partial and integral thermodynamic properties of wüstite [31].

By comparison of calculated and experimental entropy values, **Todd and Bonnickson**, and **Humphrey, King and Kelley** deducted that the lacunary iron lattice envisaged by Jette and Foote was ordered [30] [32] [33].

Brynestad and Flood observed that some (electron holes) Fe^{3+} are necessarily located in tetrahedral sites written as $[Fe^{III}O_4]$ [34].

Using neutron diffraction analyses, **Roth** determined the proportion of Fe^{3+} occupying the tetrahedral sites of the fcc structure and concluded to the formation of clusters (2:1) constituted of two iron vacancies and one tetrahedral site occupied by a cation Fe^{3+} [35]. Tarte *et al.* also showed directly by I.R. spectroscopy the existence of these $Fe_{i}^{\circ\circ\circ}$ ions [36].

Using the formalism of the mass action law initially proposed by Carl Wagner *et al.* [37] [38], Brynestad and Flood [34], and subsequently **Smyth** [39] established a simplified expression linking the composition z to the equilibrium oxygen pressure as:

$$z \propto p'^{\,1/S} \qquad (2)$$

In a first attempt, Smyth characterized the defect structure of both $Mn_{1-z}O$ and $Fe_{1-z}O$ based on the experimental compositional data from Darken and Gurry [31]. His work often referenced has been continued by many authors in different areas of the defect chemistry, particularly the study of the clustering.

2.2. *Modifications or pseudo-phases W1, W2, W3*

2.2.1. Raccah-Vallet*'s team*

During years 1962-65, three supposed « allotropic varieties » or « modifications » noted Wi (i=1,2,3) named later « subphases » and then « pseudo-phases » by other authors are discovered by **Raccah** (doctoral thesis [40]), Vallet, and Kléman additionally [41-45] from their experimental measurements. An initial layout of the corresponding phase diagram is proposed, based on coordinates (Θ °C, x) [26].

During their studies from 1961 to 1989, **Vallet** *et al.* establish correlations between mass variation, *i.e.*, departure from stoichiometry expressed by x in FeO_x, temperature T and oxygen partial pressure p′ under equilibrium (see also [3]). They describe the phase diagram of wüstite FeO_x above 911°C through the following three equations connecting log p′ noted l' with the composition x and temperature T, and expressing the three thermodynamic behaviors or pseudo-phases W1, W2 and W3, successively [29]:

W1 : $\qquad l' = (46753.4T^{-1} - 7.3781).x + (-78825.3T^{-1} + 16.0613) \qquad$ (3a)

W2: $\qquad l' = (- 9568.9T^{-1} + 31.1728).x + (- 18413.3T^{-1} - 25.2569) \qquad$ (3b)

W3: $\qquad l' = (- 33238.9T^{-1} + 48.3669).x + (6883.9T^{-1} - 43.5669) \qquad$ (3c)

To better relate the nonstoichiometry and equilibrium pressure p′ to the presence of defects (mainly cation vacancies and interstitials), we have expressed l' as a function of z instead of x and we have reported l' as a function of log z values. It can be recalled that these relationships derive from the general expression of equilibrium constants K(T) linking the composition z to the oxygen partial pressure p′, following the basic setup:
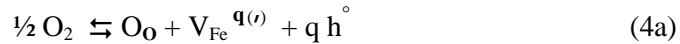
$$\tfrac{1}{2} O_2 \leftrightarrows O_O + V_{Fe}{}^{q(\prime)} + q\, h^\circ \qquad (4a)$$
$$\text{with } [h^\circ] = q.[V_{Fe}{}^{q(\prime)}] = q.z,$$
$$K(T) = \{[O_O].[V_{Fe}{}^{q(\prime)}].[h^\circ]^q\} / (p')^{\frac{1}{2}} = C.(z^s / p')^{\frac{1}{2}} \qquad (4b)$$
$$\Rightarrow \qquad \log z = (1/s).\log(K(T)/C)^2 + (1/s)\, l' \qquad (4c)$$

where C depends on q [39]. For iron vacancies expressed V_{Fe}, exponent q(′) indicates a charge q times minus; h° correspond to an electron hole. In the expression of K(T), we have neglected the activity coefficients, considering that they are slowly varying with z in a limited composition range. The activity $[O_O]$ of oxygen on its site fcc is considered equal to 1 because no significant amount of vacancies can be present in the oxygen lattice. Finally, we have taken into account the relationship -q.$[V_{Fe}{}^{q(\prime)}]$+$[h^\circ]$ = 0 (electroneutrality condition) with $[V_{Fe}{}^{q(\prime)}] = z$.

The equilibrium constants depend on the values 2, 1, and 0 of q. The three hypothetical corresponding values of exponent s should be 6 (q=2), 4 (q=1), and 2 (q=0) (more likely close to these values, taking into account the various approximations made). In the remainder of this review,

exponent s is taken as characteristic of the specific equilibrium equation connecting the fractions of point defects between them.

Let us note that the relationships between activities and compositions z are not strictly linear. They assume the existence of three domains and allow a comparison with classical models of defect equilibria. In each domain, a unique model of defect equilibrium is supposed to be valid, which is not strictly exact because of the continuous evolution of interactions between defects, as composition and temperature vary in the phase diagram.

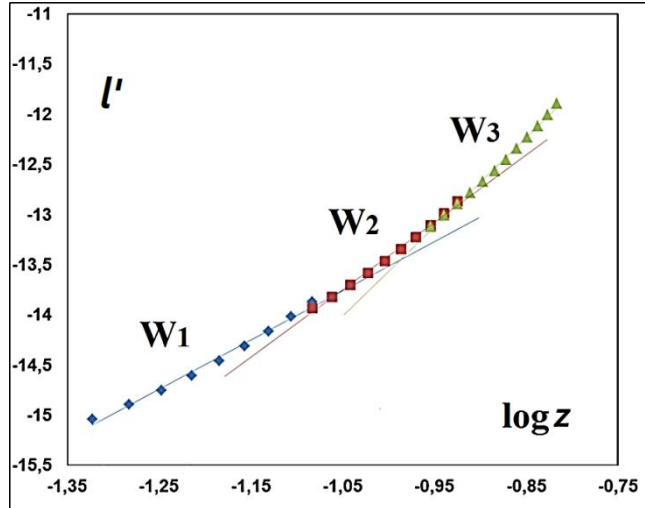### 2.2.2. Fixed temperature and variable composition

To illustrate the different behaviors or transitions between one and another in Fig. 1 below, we detail the relation $\log z$ *vs* l' (see relationship 4c) in the specific case of the Vallet *et al.* data, as obtained at 1000 °C (T=1273 K), using the relationships (3a, b, c) above, and transforming them into the following relationships:

W1: $\quad\quad\quad\quad\quad\quad \log z = 0.2036\, l' + 1.7511 \quad \rightarrow \quad s = 4.9\ (\pm 0.10)$ (5a)

W2: $\quad\quad\quad\quad\quad\quad \log z = 0.1369\, l' + 0.8352 \quad \rightarrow \quad s = 6.7\ (\pm 0.12)$ (5b)

W3: $\quad\quad\quad\quad\quad\quad \log z = 0.1124\, l' + 0.5246 \quad \rightarrow \quad s = 8.9\ (\pm 0.15)$ (5c)

From the three segments observable on the curve l' *vs* $\log z$ in Fig. 1, we can derive three different values: s(W1) = 4.9, s(W2) = 6.7, and s(W3) = 8.9. These values are similar to the ones found by Toft Sørensen and El Sayed Ali, and Rekas and Mrowec [46] [47]. In reality, there is no reason for assuming linear relationships given the probable existence of mixtures of defects, and of their continuous evolution conditioned by the changes in charge of $V_{Fe}^{q(')}$ (q=0,1,2).

Fig. 1. The logarithm l' of oxygen partial pressure p′
***vs* the logarithm of composition z**
derived from the data [29] at 1273 K.

2.2.3. Fixed composition and variable temperature

For a fixed value $x = 1.130$ ($z = 0.115$), we report in Fig. 2 the experimental values of l' versus 1/T using the data of Vallet and Carel [29]. Three quasi linear domains can be distinguished suggesting the existence of three Gibbs free energies of reaction in relation with the equilibrium constant K(T), with the classical relationship $\Delta G(reaction) = \Delta H - T\Delta S = -RT\ln K$. The linear correlations are:

W1: $\quad\quad\quad\quad\quad\quad l' = -2.5994(10^4.T^{-1}) + 7.724$ (6a)

W2: $\quad\quad\quad\quad\quad\quad l' = -2.9226(10^4.T^{-1}) + 9.9684$ (6b)

W3: $\quad\quad\quad\quad\quad\quad l' = -3.0676(10^4.T^{-1}) + 11.088$ (6c)

Using the simplified relationship (4b) without activity coefficients, we can derive the following relations for the fixed value $z = 0.115$ following:

$$\log K(T) = (s/2).\log z - \tfrac{1}{2} l' + \log C = - (2/2.3026) \Delta G/RT \quad (7a) \quad \blacktriangleright \quad dl' / d(1/T) = (2/2.3026) \Delta H/R \quad (7b)$$

From relation (7b), three values of enthalpies can be determined, linked to the changes in slopes and attributable to the pseudo-phases:

W1: $\qquad\qquad \Delta H_1/R = - 25526$ K $\quad \longrightarrow \quad \Delta H_1 = - 2.20$ eV

W2: $\qquad\qquad \Delta H_2/R = - 29322$ K $\quad \longrightarrow \quad \Delta H_2 = - 2.52$ eV

W3: $\qquad\qquad \Delta H_3/R = - 31008$ K $\quad \longrightarrow \quad \Delta H_3 = - 2.67$ eV
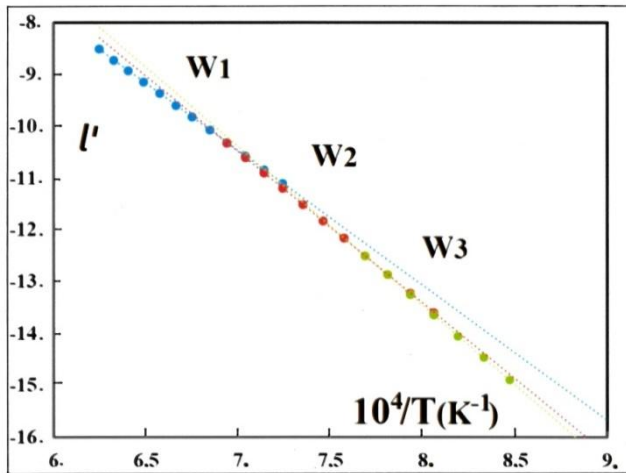
Fig. 2. Variation of l' vs 1/T for a fixed value $z = 0.115$: three quasi linear correlations corresponding to the initial determinations in the three domains W1 (high T), W2 (intermediate T) and W3 (low T) give rise to three activation energies ΔH_i.

At the same time, a qualitative dilatometric study under CO2/CO indicates weak changes of slopes in curves $\Delta l(T)$ with intersections located on the boundary W2/W3 [48]. In addition, several correlations between the cubic cell parameter obtained after quenching or *in situ* and the composition x in FeO_x led correspond to the separation in three pseudo phases or subdomains of the equilibrium phase diagram [49] [50].

In the equations above, we have neglected the activity coefficients, assuming that the ionic interactions remained constant as z varies. Another point of view would be to consider that a significant evolution of the activity coefficients can be observed and that the variation is associated with molar fractions [i] of point defects at equilibrium (the activity a_i being proportional to the molar fraction: $a_i = \gamma_i .[i]$). In the case of ionic solids, these activity coefficients γ_i are generally used to express deviations from ideal models of isolated defects at equilibrium.

2.3. Abnormal behavior near 1184/1185 K
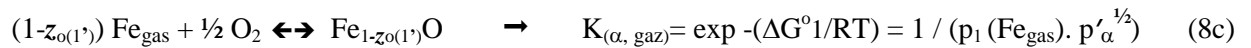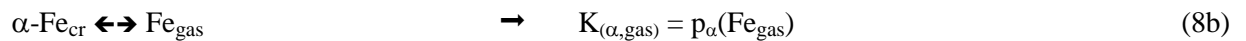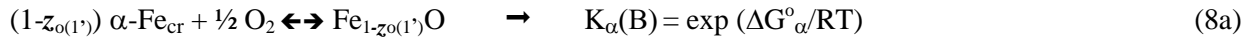
2.3.1. A splitting of the phase diagram

Vallet proposes a separation of an upper subdomain W of the phase diagram from the lower subdomain W' on each part of the first order transformation α-Fe $\leftrightarrows$ γ-Fe [51]. Each subdomain is constituted of three pseudo-phases W'j below and Wi above 1184 K. Because the properties of W' and W are distinct, the boundaries with α- or γ-iron of the stability domains are also distinct. That is the reason for the existence of points B and A, at the upper and lower end respectively of the corresponding curves in the phase diagram (see [28], lines at 1184.15 K in Tables IV and V p. 723 and 724). The limit compositions on these boundaries $y_{o(1)}$ = 0.9427 or $z_{o(1)}$ = 0.0573, and $y'_{o(1')}$ = 0.9528 or $z_{o(1')}$ = 0.0472 of W1 and W'1 in equilibrium with γFe-O_ε and αFe-$O_{\varepsilon'}$ are proposed at points A and B, respectively, both assumed at 1184 K, which cannot strictly occur as discussed below.
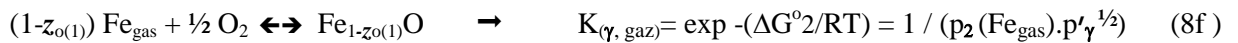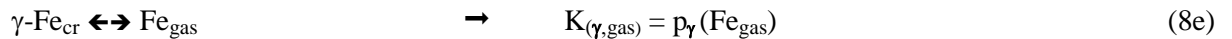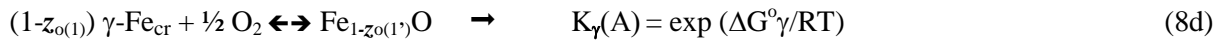
5

2.3.2. Thermodynamic inconsistency

In an extended and careful review published in 1991, **Wriedt** [17] asks questions about the isotherm at 1184 K, and its assumed continuity, while it seems to correspond with transitions Wi/W'j, *i.e.*, with five sub-boundaries for the indexes 1/1, 2/1, 2/2, 2/3 and 3/3. Are they linked to the α-γ Fe transformation? These pending questions have no answer until the 1980s.

The basic equations governing the various equilibria between gases and solid phases (see equilibrium diagram in Fig. 3) are listed below. Particularly at the two boundaries involving α-Fe_{cr} or γ-Fe_{cr} (subscript 'cr' for 'solid', *i.e.*, 'crystallized'), equilibria can be expressed:

1) on the boundary αFe/W'₁ from point B to point C,

$$(1-z_{o(1')})\ \alpha\text{-}Fe_{cr} + \tfrac{1}{2}\,O_2 \longleftrightarrow Fe_{1\text{-}z_{o(1')}}O \qquad \longrightarrow \qquad K_\alpha(B) = \exp\,(\Delta G^o{}_\alpha/RT) \qquad (8a)$$

$$\alpha\text{-}Fe_{cr} \longleftrightarrow Fe_{gas} \qquad \longrightarrow \qquad K_{(\alpha,gas)} = p_\alpha(Fe_{gas}) \qquad (8b)$$

$$(1-z_{o(1')})\ Fe_{gas} + \tfrac{1}{2}\,O_2 \longleftrightarrow Fe_{1\text{-}z_{o(1')}}O \qquad \longrightarrow \qquad K_{(\alpha, gaz)} = \exp\,\text{-}(\Delta G^o 1/RT) = 1 / (p_1\,(Fe_{gas}).\,p'_\alpha{}^{1/2}) \qquad (8c)$$

2) similarly, on the boundary Feγ/W1 from point A to melting,

$$(1-z_{o(1)})\ \gamma\text{-}Fe_{cr} + \tfrac{1}{2}\,O_2 \longleftrightarrow Fe_{1\text{-}z_{o(1')}}O \qquad \longrightarrow \qquad K_\gamma(A) = \exp\,(\Delta G^o{}_\gamma/RT) \qquad (8d)$$

$$\gamma\text{-}Fe_{cr} \longleftrightarrow Fe_{gas} \qquad \longrightarrow \qquad K_{(\gamma,gas)} = p_\gamma\,(Fe_{gas}) \qquad (8e)$$

$$(1-z_{o(1)})\ Fe_{gas} + \tfrac{1}{2}\,O_2 \longleftrightarrow Fe_{1\text{-}z_{o(1)}}O \qquad \longrightarrow \qquad K_{(\gamma, gaz)} = \exp\,\text{-}(\Delta G^o 2/RT) = 1 / (p_2\,(Fe_{gas}).\,p'_\gamma{}^{1/2}) \qquad (8f)$$

At the arbitrarily unique temperature of 1184 K, it is thus necessary to apply two different partial pressures p_1 and p_2 of Fe(gas), at equilibrium with the solid at points A and B. Obviously, at the unique $\alpha \leftrightarrows \gamma Fe$ equilibrium temperature, it exists only one value of the pressure $p(Fe_{gas}) = 3.005 \times 10^{-11}$ atm. Thus, the points A and B cannot be at the same temperature. Correlatively, in the case of the points A and B differing in temperatures T(A) and T(B), the compositions $z_{o(W)}(A)$ and $z_{o(W')}(B)$, the equilibrium partial pressures $p'(A)$ and $p_2(A)$, $p'(B)$ and $p_1(B)$ of oxygen and iron gas are necessarily different. Finally, a small difference in temperatures, probably a few degrees, are to be determined experimentally in order to adjust this set of parameters, which determines the phase diagram (Fig.II-3) close to the stable temperature of the α-γFe transition. In this situation, the bottom row in Table IV should be changed to a value of T(A) higher than 1184/1185 K, and the header line of Table V to a value of T(B) also higher than 1185 K, but lower than T(A) in ([28] p. 723 and 724).

Note: If T(A) and T(B) differ from a typical value of 4 °C (see *2.3.4. Fe-O phase diagram close to 1185 K*), for example T(A) = 1191 K and T(B) = 1187 K, the partial pressures of iron are necessarily $p(A)=p_1=3.692 \times 10^{-11}$ atm and $p(B) = p_2 = 3.220 \times 10^{-11}$ atm following tabulated data [52], [53], [54]. Thus, the differences between the two iron partial pressures is on the order of 0.4×10^{-11} atm. The corresponding partial pressures of oxygen are $p'(A) = 4.829 \times 10^{-17}$ atm and $p'(B) = 4.229 \times 10^{-17}$ atm, *i.e.* a difference of 0.6×10^{-17} atm. The compositions $z_o(A) = 0.0571$ and $z_o(B) = 0.0468$ correspond to a gap of ~0.01 in composition.

2.3.3. Phenomena observed close to the isotherm at 1185 K

Experimental confirmations of this hypothetical separation exist in the literature. Several of them are interesting to be examined. Löhberg and Stannek separate the pre-exponential term a and the energy term b = $\Delta G/RT$ of an expression functionally similar to a Boltzmann distribution $p_{H2O}/p_{H2} = a.\exp(b.z)$ expressed as a function of T^{-1} in two segments intersecting in the vicinity of the $\alpha \leftrightarrows \gamma Fe$ transition temperature in ([55] Fig. 8 and 9 p. 250).

Similarly, Janowski, Mrowec, Stokłosa separate in two segments the variation of the self-diffusion coefficient D^*_{Fe} of iron in wüstite as a function of T^{-1} from their own results and several sets from the literature in ([56] Fig. 7 p. 99). The intersection occurs for $T^{-1} = 8.28 \times 10^{-4}\ K^{-1}$, *i.e.,* at 935°C, of the segments attributed to W and W'.

Jacobsson and Rosén, Guillermet and Per Gustafson, Sjödén, Seetharaman and Staffanson, Grønvold *et al.* publish new experimental thermodynamic data of highly improved accuracy about the molar thermodynamic properties of iron and wüstite [57] [58] [59] [60].

Sundman, in an assessment of the entire Fe-O system, formulate a model for the 'pure iron corner' (solid solutions γFe-O$_\varepsilon$ and αFe-O$_{\varepsilon'}$) [16]. The assessment of Spencer and Kubaschewski is also relevant in the same context [7].

A departure from a monotonous variation of the electromotive force of galvanic cells, near the $\alpha \leftrightarrows \gamma$Fe transition, is evidenced from measurements at the iron/wüstite electrode, in several galvanic cells [57] [59]. In addition, authors [59] publish their numerous determinations of the electromotive force (e.m.f.) between 866.7 and 1339.3 K. An anharmonic transitional zone between two separate continuous variations, not in continuation of each other, can be identified in the temperature range [1186-1194 K].

2.3.4. Consequences relevant to the Fe-O phase diagram

The $\alpha \leftrightarrows \gamma$ Fe first order transition in the 'pure iron corner' of the phase diagram Fe-O is not documented sufficiently. The left side in Fig. 3 displays literature data (relative to FeO$_x$) concerning the domain of this transition [7] [16] [61]. The temperature of the strictly pure αFe$\leftrightarrows\gamma$Fe transition is tabulated at 1184 ± 3 K in the data base NIST-Janaf (1999-2011) [54]. At present, it is generally taken to be 1185 K (point ø in Fig. 3).
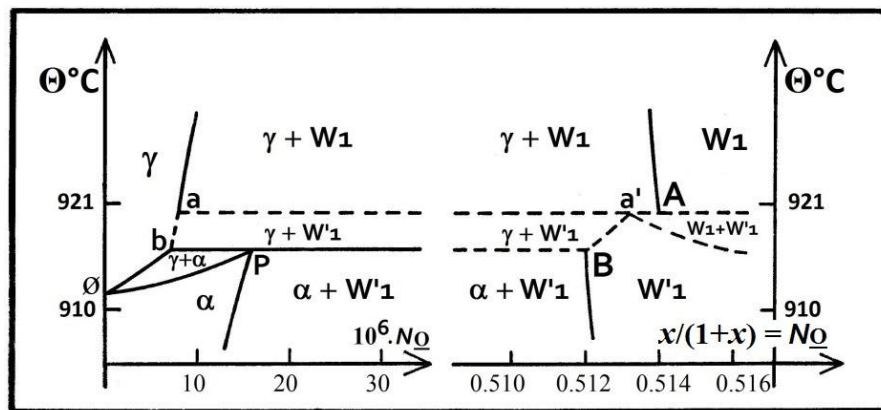
Fig. 3. Equilibrium diagram (FeO$_x$) between W1 and W'1 and 'pure iron', with both limit points A and B of γ-Fe/W1 and α-Fe/W'1 boundaries. Compositions $N_{\underline{O}} = x/(1+x)$ are arbitrarily taken at 1184 K in paper [28]. Dashed lines correspond with hypothetical limits.

The $\alpha \leftrightarrows \gamma$ Fe transitional enthalpy is known with a twenty percent dispersion from assessed and experimental data, (see [58] Table 3 p. 604). Very few experimental studies are available concerning the P(eritectoid) invariant point (αFe-O$_{\varepsilon'}$, W'1, γFe-O$_\varepsilon$) close to the temperature of the pure α-Fe $\leftrightarrows$ γ-Fe transition [61]. Sundman takes up the molar fractions ($\cong \varepsilon$ at point P, ε' at point b in Fig. 3) of dissolved oxygen $N_{\underline{O}} = x/(1+x)$ = 16 x 10^{-6} and 6.8 x10^{-6} in α- and γ-Fe respectively at 1185 K or 912 °C [16] (Fig. 3).

The separation of the boundary iron/wüstite into parts γFe-O$_\varepsilon$/W1 from point A and αFe-O$_{\varepsilon'}$ /W'1 from point B arises distinctly in the temperature range characterized in [59], following the suggested phase diagram in the right part of Fig. 3. Two types of two-phase domains (γ + W'1) and (W1 + W'1) have been added hypothetically as well as an invariant point a' (W'1, γFe-O$_\varepsilon$, W1). As of now, the location of points A and B remains to be determined precisely. New experimental data is necessary to confirm the preceding suggestions.

For the subdomain of W' below 912 °C, the information equivalent to that of W above 912 °C is more difficult to access (see [44] Figs. 6 and 7 p. 12 and 13). An empirical relationship associated with the three W'j requires a curvature term. The analytical expression has been taken as follows:

$$l' = (a'_j T^{-1} + b'_j) \, x^2 + (c'_j \, T^{-1} + d'_j) \, x + (e'_j \, T^{-1} + f'_j) \qquad (9)$$

The corresponding coefficients (a'$_j$ - f'$_j$) are available numerically in ([29] Table 1 p. 210).
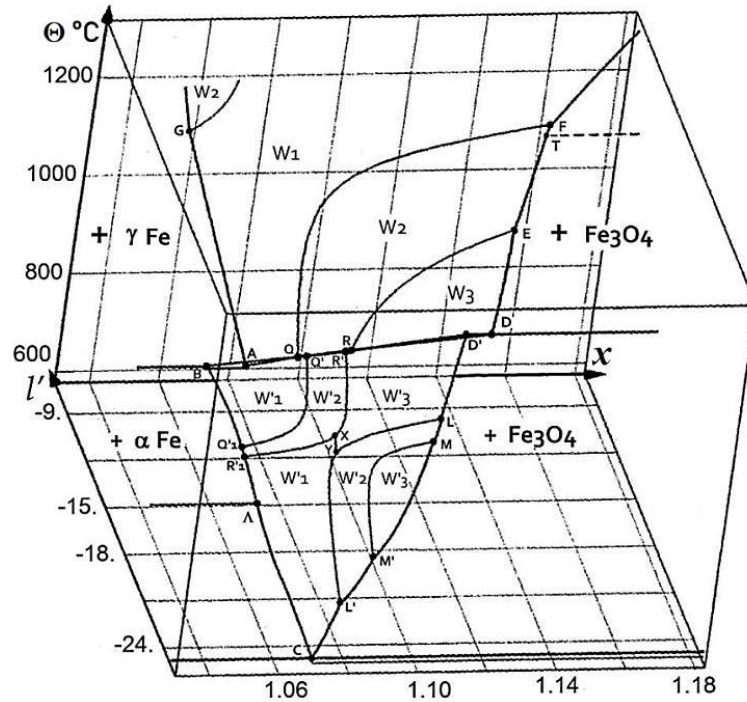
Fig. 4. Phase diagram Θ °C (l', x) of solid wüstite FeO$_x$ under equilibrium following Raccah-Vallet-Carel; upper temperature 1250 °C, lower one 592 °C at point C; coordinate l' for $\log_{10}p(O_2)$. Points noted by a capital letter are tabulated in [27], except the point Λ in [28] and the point T in [62] [63] [64].

The sets of numerical relations detailed above for l' as functions of x and T^{-1} allow the determination of the transition lines or boundaries between domains of the pseudo-phases W1, W2 and W3, from γ-iron to magnetite between 912 and around 1400 °C, and W'1, W'2 and W'3, from α-iron to magnetite between 912 and 592 °C, at point C, as drawn in Fig. 4 (see precedent drawings [26] [27] [29]).

2.4. First evidences of phase modifications or pseudo-phases in the literature

2.4.1. Wagner jr's team

In the course of (thermodynamics - defect structure) approaches by Carl Wagner, **Wagner jr** et al. study the electrical conductivity σ at equilibrium as function of log p$_{O2}$ [65]. With the help of their own thermogravimetric data $l'(x)$ [66], they state that the composition of the break on their curves σ(x) well agree with that of the transitions Wi ⇆ Wi+1 determined in Raccah's work. So, the pseudo-phases are identified at equilibrium outside of Vallet's group for the first time (see [65] Table IV p. 955; also Annex A Fig. A1 a-). The further studies of Wagner jr's group about wüstite were concerned with transport phenomena in the bulk and on the surface, in relation with the p to n transition.

2.4.2. Fender and Riley

From numerous accurate electromotive force measurements (e.m.f.) in galvanic cells, **Fender** and **Riley** [67] brought the second experimental confirmation, outside of Vallet's team, of the likely existence of

three pseudo-phases, and the location of the boundaries of the subdomains in the range 700-1350 °C. Their plot of the equilibrium diagram is in fairly good agreement with that of Vallet *et al.* (see Annex A, Fig. A2).

2.5. Partial molar enthalpies and entropies. Convergence point Ω

Fender and Riley, then later Vallet and Carel assessed the partial molar properties of an oxygen solid solution ($\Delta \overline{H}_{\underline{O}} \equiv \overline{H}_{\underline{O}} - \frac{1}{2} H^{\circ}_{O2}$, $\Delta \overline{S}_{\underline{O}} \equiv \overline{S}_{\underline{O}} - \frac{1}{2} S^{\circ}_{O2}$) as functions of $x \in [1.058 - 1.172]$ for the three pseudo-phases Wi (i=1,2,3) named also wI, wII and wIII (see [67] Table I p. 796, and *infra* in Figs. 5 and 6). The following relations were formulated in [28] for the three Wi (i=1,2,3) at T >1184 K:

$$\Delta \overline{H}_{\underline{O}} = 19.14475(a_i.x + c_i), \qquad (10h)$$
$$\Delta \overline{S}_{\underline{O}} = -19.1447 (b_i.x + d_i) \qquad (10s)$$
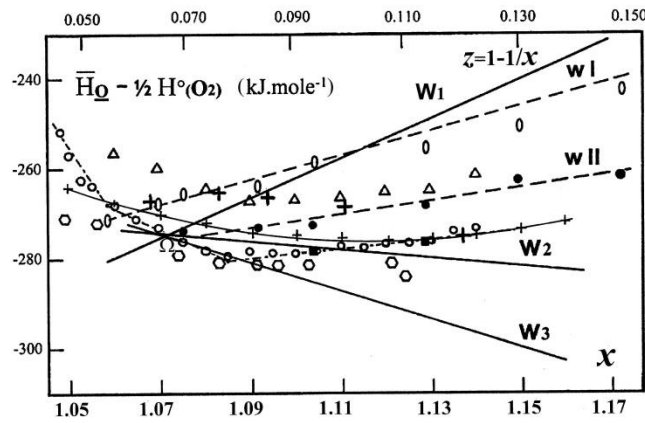
Fig. 5. $\Delta \overline{H}_{\underline{O}}$ **from some authors.** — **: derived for the Wi (i=1-3) *i.e.* at T $\in$[1193 - 1523 K] from thermogravimetry + CO2/CO [28]; 0--0: w I, •--• : wII, and ■: wIII (two points only) by emf at T$\in$[1023-1623 K] [67]; dash-dot line O----O: by calorimetry at 1348 K under vacuum (+ δn_{O2}) [68]; ✛: by emf at T$\in$[873-1273 K] [69]; △: by thermogravimetry + CO2/H2 at T $\in$[1373-1673 K] [70]; O: by emf at T $\in$[823-1323 K] [71]; +: by emf data at T $\in$[873-1373 K] [72] [13].**

and, for the three W'j (j=1,2,3) at T< 1184 K:

$$(\Delta \overline{H}_{\underline{O}})' = 19.14475 (a'_j.x^2 + c'_j.x + e'_j) \qquad (11h)$$
$$(\Delta \overline{S}_{\underline{O}})' = -19.14475 (b'_j.x^2 + d'_j.x + f'_j) \qquad (11s)$$

Relations (10) for the Wi, and (11) for the W'j are independent of T, in accordance with the property of regularity ([12] p. 81-85) of the solid solution wüstite identified in [41] but contested in [68]. $\Delta \overline{H}_{\underline{O}}$ is represented in Fig. 5 from numerous available data sets. A convergence in the vicinity of the common intersection point Ω at $x = 1.0713$ (± 0.001) of the straight lines $\Delta \overline{H}_{\underline{O}}(x)$ from (10h) is globally noticeable.

Contrary to this contrived amalgamation process, the numerical adjustments presented next are related principally to the initial results from Raccah [40] to [44] which form a well populated and coherent data set at equilibrium, and for which it exists now a systematic interpretation by Vallet's group [27] [28] [29], and experimental confirmations [65] [67] [73].

The graphical representation of the relations (10h) and (11h), (10s) and (11s), in the case of the isotherms at 1000 and 820 °C, is given in Fig. 6. Along the isotherm at 1000 °C, the three Wi are represented by successive linear segments. For the two transitions Wi →Wi+1 at decreasing iron content, a jump is observed toward the lower molar heat and entropy of solution which are exothermic and exo-entropic. For $x_{1/2}$ = 1.0782: $\delta(\Delta \overline{H}_{\underline{O}})$ = -3.5 kJ, $\delta(\Delta \overline{S}_{\underline{O}})$ = -2.3 J. K^{-1}, and $x_{2/3}$= 1.1154: $\delta(\Delta \overline{H}_{\underline{O}})$ = -10.5 kJ, $\delta(\Delta \overline{S}_{\underline{O}})$ = -8.3 J.K^{-1}.

Above 1184 K, the exothermic $\Delta \overline{H}_{\underline{O}}$ for W1 increases with x and z corresponding to oxygen dissolution. For each $\underline{O}$ a vacancy and zero, one or two electronic holes are created simultaneously as the

clustering is in progress (see equation (4a)). For W3, $\Delta\bar{H}_O$ is decreasing with x, probably because of the formation of long-range ordering. For W2, $\Delta\bar{H}_O$ varies in a manner intermediate between that for W1 and W3, which corresponds to the observation that W2 is a solid solution of W1 and W3 [67].
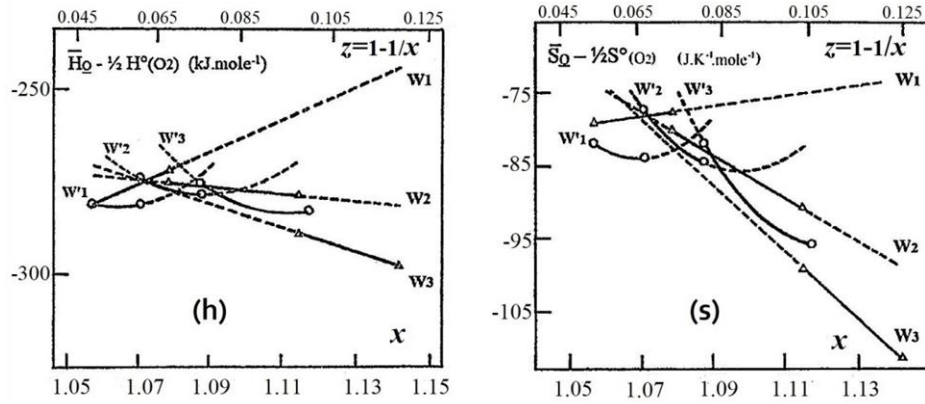
Fig. 6. Partial molar enthalpy ($\bar{H}_O$ - $\frac{1}{2}H^\circ_{O_2}$) and entropy ($\bar{S}_O$ - $\frac{1}{2}S^\circ_{O_2}$) of solution of oxygen, through the stability field of wüstite, whatever the temperature. Transitional jumps are at 820 °C (W'i) and 1000 °C (Wi). Dashed lines are drawn in extrapolated or metastable zones.

Along the isotherm at 820 °C, the three W'i are represented by parabolic curves. Jumps (weaker in amplitude than the ones at 1000 °C) are observed toward higher values for the molar exothermic transitions W'j→W'j+1, $x_{1'/2'} = 1.071$: $\delta(\Delta\bar{H}_O)' = +10.9$ kJ, $\delta(\Delta\bar{S}_O)' = +6.3$ J.K^{-1} and $x_{2'/3'} = 1.1154$: $\delta(\Delta\bar{H}_O)' = +2.9$ kJ, $\delta(\Delta\bar{S}_O)' = +2.7$ J.K^{-1}. A convergence of parabolas $\Delta\bar{H}_O'(x)$ is observed for $x = 1.0852$ or $y = 1-z = 0.9215$ (± 0.004). This convergence occurs for a composition different ($\delta y = 1.3 \times 10^{-2}$) from that of point C ($y = 0.935$), and is not defined as precisely for W' as it is for W.

The Gibbs-Duhem relation leads to the iron solution property $\Delta\bar{H}_{Fe}$ from $\Delta\bar{H}_O$ (Fig. 7).
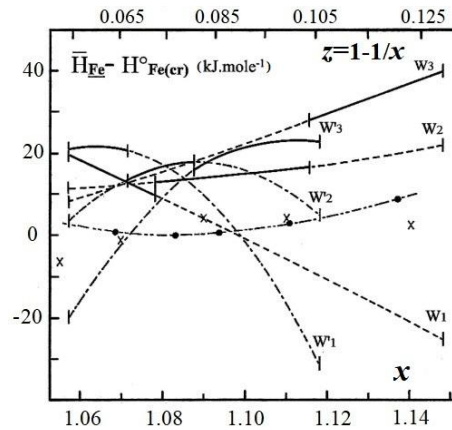
Fig. 7. Variations of the partial molar enthalpy ($\bar{H}_{Fe}$ - H°_{Fe}) vs x for the isotherms at 1000 °C (Wi) and 820 °C (W'j). For comparison: ●--●: $\Delta\bar{H}_{Fe}$ from e.m.f. measurements at 1000 °C by Asao et $al.$ ([69] Table 3 p. 75); ×: Darken and Gurry determinations ([31] Table X p. 1408).

In the domain of W, exothermic transitional jumps are observed toward the higher values for the two transitions Wi → Wi+1 at equilibrium. At 1000 °C, the transition W1/W2 ($x_{1/2} = 1.0782$) is characterized by $\delta(\Delta\bar{H}_{Fe})_{1/2} = 3.25$ kJ.mol^{-1}, $\delta(\Delta\bar{S}_{Fe})_{1/2} = 2.56$ J. K^{-1}.mol^{-1}. The transition W2/W3 ($x_{2/3} = 1.1164$) is characterized by $\delta(\Delta\bar{H}_{Fe})_{2/3} = 12.06$ kJ.mol^{-1}, $\delta(\Delta\bar{S}_{Fe})_{2/3} = 9.47$ J.K^{-1}.mol^{-1}. In the domain of W', the equivalent jumps are exothermic as shown in Fig. 7 drawn for transitions at 820 °C.

As iron deficiency increases, the partial molar enthalpy of solution of iron $\Delta\overline{H}_{Fe}$ decreases for W1 and increases for W3, variations that are opposite to that of $\Delta\overline{H}_O$. The five determinations of Asao *et al.* at 1000 °C are distributed on a curve noticeably parallel to the set of the successive segments concerning W1, W2 and W3 [69].

Equations $x_{i/i+1}(T)$ of the lines -the so-called boundaries- separating the domain of stability of single pseudo-phases Wi and Wi+1 were adjusted following the analytical equations:

$$x_{i/i+1} = [(c_{i+1} - c_i) + T.(d_{i+1} - d_i)] / [(a_i - a_{i+1}) + T.(b_i - b_{i+1})]$$

(see [26] p. 3680, equations (6)). Numerically, they are adjusted now to

$$x_{1/2} = (60412.0 - 41.3182T) / (56322.3 - 38.5509T) \tag{12}$$
$$x_{2/3} = (25297.2 - 18.310T) / (23670.0 - 17.1941T) \tag{13}$$

A metastable boundary can also be envisaged

$$x_{1/3} = (85709.2 - 59.6282T) / (79992.3 - 55.7450T) \tag{14}$$

The authors in [43] remarked that the corresponding terms in the numerator and the denominator [of equations (12), (13) and (14)] are almost exactly proportional in a same ratio of 1.07, *i.e.*, $(c_{i+1} - c_i) / (a_i - a_{i+1}) = (d_{i+1} - d_i) / (b_i - b_{i+1}) \cong 1.07$, also close to Chaudron's point composition. It results that the three pseudo-phases are under equilibrium at T (K) under the same oxygen pressure for a composition $x \cong 1.07$ (*e.g.*, p′ $\cong 8$ $\times 10^{-17}$, $4\ 10^{-15}$ or 8×10^{-11} atm at 1184, 1273, or 1573 K respectively), irrespective of index i. This result constitutes the reason why the property $\Delta\overline{H}_O$ (= -274.8 kJ.mol^{-1}) of equation (9h) is shared by the three Wi's with the same composition $x \cong 1.07$ under the same equilibrium oxygen potential. The convergence at point Ω results of that fact. The iron partial molar properties converge also for $\Delta\overline{H}_{Fe} = +87.8$ kJ.mol^{-1} at 1000 °C. At invariant point C (α-Fe, W'1, Fe3O4) of abscissa $x_C = 1.070_0$, these properties are merged ($\Delta\overline{H}_O = -290.4$ kJ.mol^{-1} and $\Delta\overline{H}_{Fe} = +21.4$ kJ.mol^{-1}).

It is noticeable that a common « kinetic origin » ω is characterized by $x = 1.070 \pm 0.001$ in W' (see Annex 2 « Re-analysis of kinetic data at 850 °C», derived from the experimental results [73]).

2.6. The triple point (W1, W2, W3) out of equilibrium

The point 8 (W1, W2, W3) was determined as the intersection of the extrapolated boundaries W1/W2 and W2/W3 at temperature 302 °C and composition $y = 0.9322$, directly below point Ω and point C ($y_C \cong 0.935_0$) (see [26] Table III and Fig. p. 3681).

Manenc *et al.* observed a disproportionation near 300 °C, in a miscibility gap, by inducing a slow drop in temperature [74-75]. Fender and Riley remarked that wII ($\equiv$W2) behaves $[\partial(\Delta\overline{G}_O\ vs\ 1-x)/\partial T]$ in its specific region as a two-phase system above its critical temperature. Similarly to Vallet and Raccah [26], they remarked that the extrapolation into the metastable domain below point C shows the phase separation into wI ($\equiv$W1) and wIII ($\equiv$W3) in the vicinity of 315 °C » [67].

As early as 1977, Andersson and Sletnes studied conjointly the ordering and the preceding behavior below 300 °C, in reference with the spinodal decomposition using electron diffraction and microscopy (dark field images) [76] [77]. Typical patterns were attributed to the phase P′ (periodicity of 2.6a$_o$), in the composition interval y (of Fe$_y$O) $\in$ [0.95-0.92]. After heat treatment for 20 min at 300 °C, a tetragonal or orthorhombic symmetry was observed which can be compared to ordered P′-type regions. For compositions less than $y = 0.91$ in Fe$_{0.91}$O ($z \geq 0.09$), the more ordered structure identified as P″ was observed even after quenching. Its parameters are a = b = c = 5a$_o$.

These different observations indicate that W2 can be represented as a solid solution of W1 and W3, consistent with the determinations of $[\Delta\overline{H}_{Fe}(x)]_i^e$ as determined below.

11

2.7. Trends to ordering at increasing z

The difference $[\Delta\bar{H}_{\underline{Fe}}(x)]_i^e$ between the partial molar enthalpy of iron in $(FeO_x)_i$ and $FeO_{x_{o(i)}}$ on the boundary with Fe was envisaged as an excess type property in order to tentatively establish links between thermodynamic and defect structure properties [45]. The corresponding relations, using the previous formalism established for $[\bar{H}_{\underline{O}}(x)]_i$, $[\bar{H}_{\underline{Fe}}(x)]_i$, $[\bar{S}_{\underline{O}}(x)]_i$ and $[\bar{S}_{\underline{Fe}}(x)]_i$ leading to Figs. II-6 and II-7 above, are simply:

$$[\Delta\bar{H}_{\underline{O}}(x)]_i^e = [\bar{H}_{\underline{O}}(x) - \bar{H}_{\underline{O}}(x_o)]_i = 19.14475(a_i/2(x - x_{o(i)})) \tag{15h}$$

$$[\Delta\bar{S}_{\underline{O}}(x)]_i^e = [\bar{S}_{\underline{O}}(x) - \bar{S}_{\underline{O}}(x_o)]_i = -19.14475(b_i/2(x - x_{o(i)})) \tag{15s}$$

$$[\Delta\bar{H}_{\underline{Fe}}(x)]_i^e = [\bar{H}_{\underline{Fe}}(x) - \bar{H}_{\underline{Fe}}(x_o)]_i = -19.14475(a_i/4(x^2 - x_{o(i)}^2)) \tag{16h}$$

$$[\Delta\bar{S}_{\underline{Fe}}(x)]_i^e = [\bar{S}_{\underline{Fe}}(x) - \bar{S}_{\underline{Fe}}(x_o)]_i = 19.14475(b_i/4(x^2 - x_{o(i)}^2)) \tag{16s}$$

Substituting the coefficients a_i, b_i and $x_{o(i)}$ on the γ-Fe/$W_{o(i)}$ boundary by their numerical values yields Table 1. The sign of the term $[\Delta\bar{H}_{\underline{Fe}}(y)]_i^e$ as well as the sign of its derivative $\partial/\partial x$ is the sign of $-a_i$. This term corresponds to the energetic effect δU on the iron lattice for the interaction between each additional $\underline{O}$ and a mole of FeO_x into which it is dissolved (at constant iron content), a vacancy and zero, one or two electronic hole(s) being created (see *supra* relations 4a-4c).

Table 1 - Variations at 1273 K of excess properties $[\Delta\bar{H}_{\underline{O}}]_i^e$ and $[\Delta\bar{S}_{\underline{O}}]_i^e$.

FeO$_x$/Fe$_{1-z}$O	$x=1.0950$ or $z=0.0868$		$x=1.1420$ or $z=0.1243$	
W1: $a_1= 46753.4$ $b_1= -7.3781$ $x_{o(1)}= 1.0572$* $z_{o(1)}= 0.0541$	$[\Delta\bar{H}_{\underline{O}}]_1^e$ 16.90	$[\Delta\bar{H}_{\underline{Fe}}]_1^e$** -18.19	$[\Delta\bar{H}_{\underline{O}}]_1^e$ 37.94	$[\Delta\bar{H}_{\underline{Fe}}]_1^e$ -41.72
	$[\Delta\bar{S}_{\underline{O}}]_1^e$ 2.67	$[\Delta\bar{S}_{\underline{Fe}}]_1^e$** -2.87	$[\Delta\bar{S}_{\underline{O}}]_1^e$ 5.99	$[\Delta\bar{S}_{\underline{Fe}}]_1^e$ -6.58
W2: $a_2= -9568.9$ $b_2= 31.1728$ $x_{o(2)}= 1.0522$ $z_{o(2)}=0.0496$	$[\Delta\bar{H}_{\underline{O}}]_2^e$ -3.92	$[\Delta\bar{H}_{\underline{Fe}}]_2^e$ 4.21	$[\Delta\bar{H}_{\underline{O}}]_2^e$ -8.23	$[\Delta\bar{H}_{\underline{Fe}}]_2^e$ 9.03
	$[\Delta\bar{S}_{\underline{O}}]_2^e$ -12.78	$[\Delta\bar{S}_{\underline{Fe}}]_2^e$ 13.76	$[\Delta\bar{S}_{\underline{O}}]_2^e$ -26.80	$[\Delta\bar{S}_{\underline{Fe}}]_2^e$ 29.41
W3: $a_3= -33238.9$ $b_3= 48.3669$ $x_{o(3)}=1.0482$ $z_{o(3)}=0.0460$	$[\Delta\bar{H}_{\underline{O}}]_3^e$ -14.90	$[\Delta\bar{H}_{\underline{Fe}}]_3^e$ 15.97	$[\Delta\bar{H}_{\underline{O}}]_3^e$ -29.85	$[\Delta\bar{H}_{\underline{Fe}}]_3^e$ 32.69
	$[\Delta\bar{S}_{\underline{O}}]_3^e$ -21.68	$[\Delta\bar{S}_{\underline{Fe}}]_3^e$ 23.24	$[\Delta\bar{S}_{\underline{O}}]_3^e$ -43.44	$[\Delta\bar{S}_{\underline{Fe}}]_3^e$ 47.57

* For $x= x_{o(i)}$, all terms are equal to zero. ** The terms $[\Delta\bar{H}_{\underline{O}}]_i^e$ and $[\Delta\bar{H}_{\underline{Fe}}]_i^e$ are expressed in kJ.mol^{-1}, and the terms $[\Delta\bar{S}_{\underline{O}}]_i^e$ and $[\Delta\bar{S}_{\underline{Fe}}]_i^e$ in J.K^{-1}.mol^{-1}.

The values of $[\Delta\bar{H}_{\underline{Fe}}]_i^e$ in Table 1 show that:

1) for W1, the internal energy U_m of the iron lattice (the term $P\Delta V_m$ is negligible compared to the contribution ΔU_m in ΔH_m) decreases as z increases, which corresponds to the exothermic formation energy of clusters (m:n) that are thus favored (see Gokcen [5] p. 241-44, and [12] p. 42-44, and Desré and Hodaj [21] p. 91-96).

2) conversely, W3 is characterized by an increase in the lattice energy, which corresponds to the completion of the cluster percolation and the formation of the superstructure (2.55a x 2.55a x 2.55a) named P″ by Manenc and characterized using HREM by Iijima [75] [78] [79].

3) likely because W2 is more than likely a solid solution of W1 and W3, the variation of U_m is intermediate.

Such trends were discussed previously by Fender and Riley when considering $\Delta\bar{G}_{\underline{O}}$ and $\Delta\bar{H}_{\underline{O}}$ in ([67] p. 797).

The positive and negative values of the term $[\Delta\bar{S}_{\underline{O}}]_i^{\mathbf{e}}$ (see Table I) correspond mainly to a vibrational entropy change in the oxygen sublattice [20] [70] [80]. In the case of the initially disordered pseudo-phase W1, the excess entropy term weakly increasing with z shows that the disorder due to the formation of point defects is predominant. Reversely, in the case of the pseudo-phase W3, increasing short- and long-range orderings would be associated with increasing z values as indicated by a strong decrease of $[\Delta\bar{S}_{\underline{Fe}}(x)]_{\mathbf{3}}^{\mathbf{e}}$. These entropy variations are related to the increasing frequency of the Fe-O bond because of larger clusters and/or an increasing degree in their percolation until completion and superstructure. The pseudo-phase W2 can be thought to appear at the starting threshold of the percolation of clusters, when the lattice becomes more rigid.

3. Several approaches of investigation

3.1. Burgmann*'s review*

In 1968, this author gathers some experimental results (electrical conductivity and transition p-to-n). Because of numerous analogies with pyrrhotine $Fe_{1-z}S$ [81], he describes tentatively the defect structure in terms of clusters (see [4] Fig. 5 p. 173). He proposes a conduction model involving the formation of an acceptor band or of new states produced by the interaction of defects as z increases. The lattice contraction at increasing z reduces the gap between the valence and conduction bands, inducing a p-to-n transition for compositions $z = 1/12 = 0.083$ at 900 °C and $z = 1/13 = 0.076$ at 1300 °C ([4], Hillegas [82]). Such an overlap is also considered later by Molenda, Stoklosa and Znamirowski [83].

3.2. Manenc*'s phases P, P′, P″*

As the most important result of a seminal work, **Manenc** describes three types of « phases » named P, P′ and P″. He characterizes them after (rapid) quenching into water using X-ray diffraction. For an iron rich wüstite ($z < 0.08$), vacancies and ions Fe^{3+} seem to be randomly distributed. This corresponds to the phase P which has a weakly incomplete NaCl-type structure alone. Other diffraction patterns of more iron deficient samples ($0.08 < z < 0.11$) have additional reflections corresponding to a cubic cell with a repeating distance $2.6a_o$. Diffuse trails parallel to <100> directions connect these reflections. These features are characteristic of the phase P′ alloyed with the phase P, and individually observed only in « oxygen rich » samples. Iron vacancies are ordered in the two phases [75, 78].

Diffraction for a heated single crystal such as $z = 0.08$ shows that a superstructure exists in the range 800-1000 °C for this composition. The phase P″ is observed in wüstite such as $z \cong 0.10$ near 300 °C and when slowly cooled, at the threshold of disproportionation yielding Fe and Fe_3O_4. New superstructure lines are then characteristic of a commensurate 5X cubic cell [75, 78].

3.3. *Mössbauer spectroscopy*

Greenwood and **Howe** [84] interpret Mössbauer spectra in modeling the asymmetrical doublet as evidencing the differing defect structures of the pseudo-phases identified by Vallet and Raccah [44], and Fender and Riley [67] at high temperature. The quenching process produces nuclei leading to Manenc phases P, P′, [(P+P′) for $z \in$[0.05-0.08], (P′) for $z \in$[0.08-0.10], and (P″) for $z > 0.10$] below point C. The phases are detectable from fine variations of quadrupole splitting resulting from cubic symmetry distortions. These distortions can be evaluated for the single cluster (4:1), and the Koch and Cohen cluster (13:4). From a sample

such as $z \cong 0.05$, the disproportionation gives rise to $Fe_{0.918}O$ (defect rich phase P′) and $Fe_{0.976}O$ (defect poor phase P), because of a mixture of the (13:4) and (4:1) clusters.

Among numerous other Mössbauer studies reviewed by Long and Grandjean [15], Romanov, Checherskaya and Tatsienko [85] [86], Hrynkiewicz *et al.* [87], **Pattek-Janczyk** *et al.* [88], this latter is of particular interest. The authors modeled the asymmetric doublet with a singlet attributed to Fe^{3+} in tetrahedral sites, and two doublets attributed to octahedral Fe^{2+} and Fe^{3+}. They associated the maximum observed in the variation of the quadrupole splitting to the p-n transition described by [89]. This transition is likely the same as the transition « metal ↔ Mott insulator » identified by Molenda, Stokłosa and Znamirowski [83].

Aldon and **Jumas** use the Mössbauer spectroscopy to evaluate precisely the reversible insertion of lithium and the effects on the local and long-range orderings of the wüstite lattice. They characterize the lithium as « an actor of electronic pressure » (see *infra* [110] in section *4.3. Nanocomposites. Epsilon-Fe*).

3.4. First electronic-structural modeling

Goodenough's *modeling* [1] is proposed as early as 1971. Considering the relations (2) associated with thermogravimetric analyses, and relation $\sigma \propto p'^{1/5}$ (17) corresponding to the conductivity [65], the result s=6 in the W1 subdomain above 1060 °C characterizes a statistical distribution of vacancies and electronic holes (Fe^{3+}), possibly corresponding to Manenc's phase P. Below 1060 °C, the changes in values of s correspond to an increasing association between vacancies and holes. In the W2 domain, triplets Fe^{3+} - V_{Fe} - Fe^{3+} are partially ordered, improving Madelung energy. Numerous (4:1) clusters which form a superstructure according to Koch & Cohen (see *infra* section *7.2. The historical cluster (13:4)* and [130]) correspond to W3. A mapping of the transfers of iron ions, and electronic exchanges is proposed as a mechanism, needing small polarons related to energy differences between the top of the valence band and an acceptor level [1]. Later, this author with Gleitzer will consider the wüstite again from the point of view of its electronic properties and crystallographic structure. They will express some doubt concerning the role of the cluster (4:1) as only building unit of larger clusters (see [11] p. 51-4).

3.5. Zvintchuk's team

In 1973, **Tchiong Tki Khong** in **Zvintchuk**'s team, in collaboration with J. Manenc, studies samples of wüstite of composition $z \in$[0.065-0.108] quenched from 1100 °C [90]. Electron diffraction reveals three forms I, II and III corresponding to the modifications wI, wII and wIII of the phase diagram by Fender and Riley [67], and to the phases P, P′, P″. A correspondence with the three Wi is specified. The authors describe a defect complex (16:6) of point symmetry m3m, formed of six tetrahedral corner sharing clusters (4:1) distributed on the six faces of an empty cube. This cluster is represented on Fig.8.


Iron vacancy V_{Fe} (octahedral site)

Interstitial Fe^{3+} (tetrahedral site)
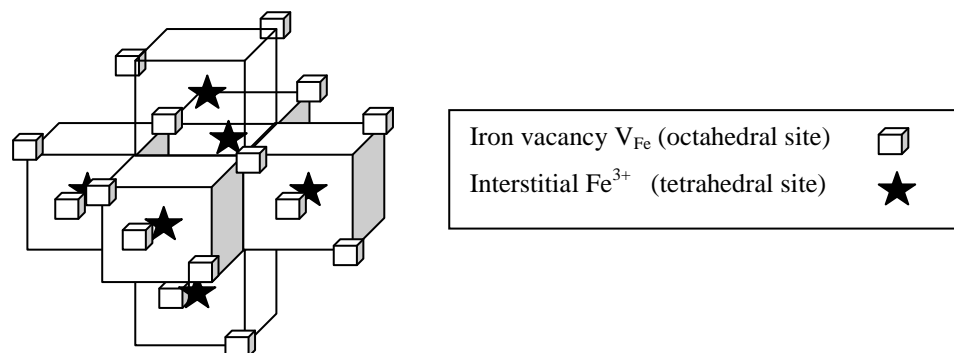
**Fig. 8. The m3m cluster (16:6) of <110> type corresponding to $(z+t)/t = 2.66$ (from ref. [90]).**

A later work by Shaïovitch, Zvintchuk and Vergazov describes a superstructure with a quadratic cell $P\bar{4}3m$ for a wüstite $Fe_{1-0.10}O$ [91].

3.6. Worral *and* Coley. *Isotopic kinetic transitions*

More than 40 years after Raccah, Vallet *et al.* [26, 41-44, 48-49], Wagner jr *et al.* [65] [66], and Fender and Riley [67], Worral and Coley evidence kinetic transitions related evidently to the pseudo-phases [73]. Following the process first used by Temkin *et al.* at the surface of iron oxides [92-93], and then applied by Grabke [94], Cramb and Belton [95], Mori, Morita and Sano [96], later by Zhang *et al.* [97] [98], Worral and Coley study the kinetics of the carbon exchange in the equilibrium W/(CO2/CO mixtures) in which a controlled proportion of $^{13}CO2$ species was introduced. In such an environment, a specific equilibrium of the carbon isotopes is established following:

$$^{13}CO_2 + CO \leftrightarrows {}^{13}CO + CO_2$$
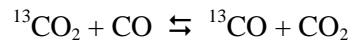
which can be viewed as the sum of the two half-reactions:

$$^{13}CO_2 \rightarrow {}^{13}CO + O_{ads} \qquad \text{and} \qquad CO + O_{ads} \rightarrow CO_2$$
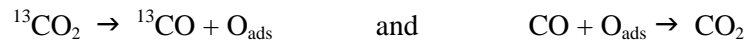
as reflecting oxygen exchange on the surface of the sample and being conditioned by the electronic structure in the bulk. The apparent rate constant is expressed as a function of oxygen activity a_O as follows:

$$k_a = k_0.a_O^{-m} \qquad \text{or} \qquad \log k_a = -m.\log a_O + \log k_0 \qquad (18)$$

The variation of $\log k_a$ with the activity a_O defined as being the ratio $p(CO_2)/p(CO)$, can be described by three successive linear segments at 995 °C, with m = 0.51 (w1), 0.66 (w2), 1.03 (w3) in ([73] Fig. 8 and equations [36] [37] [38] p. 820-1).

The authors observe only one transition attributed to two pseudo phases w'1-2 and w'3 along the isotherm at 850 °C, no change being observed in the vicinity of the forecasted boundary w'1/w'2 by Vallet and Carel [27]. The only observed transition appears as a discontinuity at the location of the transition W'2 $\leftrightarrow$ W'3 forecasted for $x = 1.090$ at equilibrium. Nevertheless, the authors state that three pseudo-phases w'1, w'2 and w'3 probably exist, but that two of them could not be separated, either because they were not detectable by electrical conductivity measurements as found before in [65], or because they were possibly « obscured by the scatter ». Finally, Worral and Coley declared that, in their study, transitions at 850 °C and 995 °C were observed « correspond[ing] exactly with the proposed pseudo-phase boundaries in quite good agreement with the phase diagram by Vallet and Carel». Because of the identity of coefficients m in the correlations concerning Wi and W'j for i=j, they attributed in a following review [22] three predominant clusters (7:2) type II to w1 and w'1, (12:4) type II to w2 and w'2 and (16:5) type I to w3 and w'3.

Note: In Annex B and Fig. B2, a graphical and numerical re-analysis of Fig. 9 by ([73] p. 821) shows a possible separation of the data in three sets at 850 °C, which correspond likely to the three W'j, provided that some data or groups of data are located in subdomains not proposed as stable. In Annex A, Fig.A1, the location of the observed transitions is represented by the set f-).

3.7. Takayama *and* Kimizuka *'s phase modifications*

Using thermogravimetric analyses under equilibrium oxygen pressure p′ defined by CO2/H2 mixtures, Takayama and Kimizuka observe significant modifications in curves representing l' *vs* $\log x$ in FeO_x [70]. The authors conclude to the existence of a transition between pseudo-phases (see [70] Table I and Annex A Fig. A1 d-). Typical changes in slopes are clearly observed from their data.
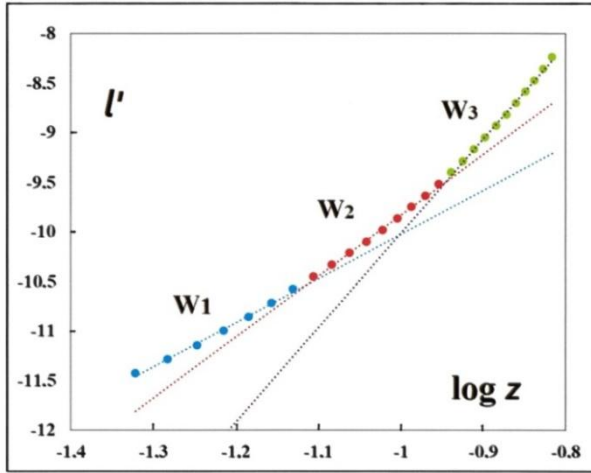
Fig. 9. Variation of l' vs $\log z$ for $Fe_{1-z}O$ at 1250 °C. Three sets of data can be defined as three quasi-linear relations.

To illustrate their results, we have transformed their representations for one temperature T=1523 K. For this temperature, their data are interpreted in terms of two relations only:

- For low x values ($x = 1/(1-z)$):

$$l' = M_1.x + B_1 = 28.512\,x - 41.366 \tag{19}$$

- For high x values:

$$l' = M_2.x + B_2 = 23.288\,x - 35.715 \tag{20}$$

The new representations for l' vs $\log z$ are done in Fig. 9. Two coefficients s can be defined as a first step, using the hypothesis of a transition implying two pseudo-phases proposed by the authors: s close to 4 and s close to 7.5. However, three correlations can be also defined as follows:

$$l' = 4.4539 \log z - 5.5685, \qquad l' = 6.1378 \log z - 3.6876, \qquad l' = 9.5059 \log z - 0.5046 \tag{21}$$

from which three values for s can be derived. A first domain for low z values yields a coefficient s = 4.5. So, it is possible to interpret the non-linear second domain in terms of two linear sequences with two coefficients s = 6.1 and s = 9.5: these two last coefficients are quite close to those obtained from the data of Vallet *et al.*

The results of Takayama and Kimizuka [70] and those of Bransky and Hed [99] show a relative agreement in the same domain of temperature (see also Annex A Fig. A1 b-), but disagree with results of Fender, and those of Vallet because these authors did not observe any breaking point on the isothermal lines above 911 °C (see *infra* section 10. Percolation approach, Nota: Metastabilities).

4. Electrical properties. Transitions. Percolation

In an extensive review about electrical properties, **Gleitzer** points out that the modeling of the electrical conductivity of wüstite is relevant of the percolation concept [19]. The superimposition of the two kinds of p-n and Wi ⇆ Wi+1 transitions, almost independent of each other, and both function of z, is already referenced in the Burgmann's review [4].

Because of this common stress, it is not easy to correlate the p-n transition to the structure. Since the percolation process is characterized experimentally by a steep variation of the studied property at a threshold composition, the curves for the electrical conductivity *vs* composition can be interpreted in terms of upgradable clusters and long-range ordering in the subdomains of W1, W2 and W3 [65] [100] [101].

Later in the present review (see Section 10 Percolation approach, Fig. 20), a statistical distribution of clusters with two types of percolation modes is schematically represented through the phase diagram. This cluster distribution can justify structurally the singularities of the integral and partial thermodynamic

properties (see above Figs. 1, 2, 5, 6, 7). Also, it can justify the distinct rate constants observed in kinetic processes (see section 3.6. *Kinetics transitions*, and Annex B: Figs. B-1 and B-2).

4.1. The p to n transition

Tannhauser observe a thermo-electronic p to n transition around 1300 °C by thermal e.m.f. analyses of a highly nonstoichiometric wüstite [89]. More precisely with Bransky [102], a change in sign of the Seebeck coefficient is observed for polycrystalline samples near O/Fe ~1.09 or z ~ 0.083 at T $\in$ [1010-1310 °C] and near z ~ 0.066 at 910 °C (Fig.10). The authors formalize the Seebeck coefficient α, in the case of completely ionized vacancies, when the hopping process is predominant:

$$\alpha = (k/e).(A/kT + \ln (c_o\text{-}c)/c) \tag{22}$$

where c = 'concentration' of charge carriers, c_o= 'concentration' of available sites for the charge carriers (see also [103]).

The same formalism is used by **Lafollet** and **Duquesnoy** in the case of non-localized when the wüstite is considered as an intrinsic semiconductor, *i.e.,* doped by its own impurities [104].

They modeled $\alpha = 0$ for $z = 0.104$ at 1100 °C, and $z = 0.108$ at 1000 °C (see [104] in Fig. 10).
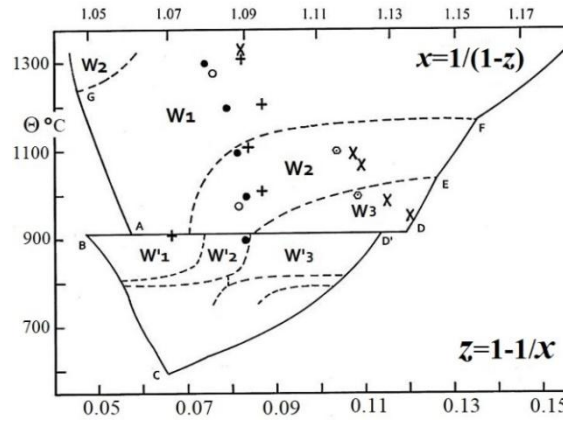
Fig. 10: Some determinations of the p-n transition by thermal e.m.f.. χ: Geiger *et al.* [66] not corrected for platinum ; +: Bransky and Tannhauser [102]; ⊙ : Lafollet and Duquesnoy [104] by modeling; o: Hillegas jr and Wagner jr [105]; ● : Gartstein and Mason [106] by re-examination of Hillegas jr's thesis [82].

Like in previous studies, **Hodge** and **Bowen** state that the experimental sign change of the thermal electromotive force, from positive to negative, occurs at increasing values of z [107]. Their model considers principally clusters (4:1) and electron holes trapped in octahedral sites adjacent to cluster vacancies. The thermally activated hopping of these holes permits continuous paths through the crystal because of the high point defect concentration between the zones separating the clusters.

In their studies on electrical conductivity, **Ariya** and **Bratch**, and **Kozheurov** and **Mikhailov** observe modifications to the relationship $\sigma \propto (p')^{1/n}$, closely related to the relationship $z \propto (p')^{1/n}$, where their coefficient n ($\equiv$ s) varied in such a way that three subdomains can be defined [100] [101]. They find an increase of the conductivity in two composition ranges, from $z \cong 0.048$ to 0.079 then from 0.079 to 0.097, in relation with the Fe/W and W/Fe3O4 boundaries.

4.2. Electrical conductivity

Neuschütz and **Towidi** establish a variation of the conductivity for T$\in$[700-1220 °C] from which they inferred that the defect electrons jumped between Fe^{2+} and Fe^{3+}, the activation energy of the process being 9.6 kJ.mol^{-1} [108].

Following **Molenda, Stokłosa** and **Znamirowski**, the conductivity can be the sum of an « extrinsic conductivity σ_y » related to the nonstoichiometry and of an « intrinsic component σ_o » independent of the defect concentration, *i.e.,* of p′ [83]. Charge transport at high temperature would occur simultaneously in the valence and conduction bands, and the dopant acceptor band due to Fe^{3+} in octahedral and tetrahedral sites. Near the composition $z \approx 0.08$, the acceptor band would overlap the valence band giving rise to a broad metallic band close to the thermoelectric transition p to n for $z \approx 0.09$ and corresponding to the stability limits of W1 and W2-3. Experimental details are given in ref. [83] (Fig. 2 p. 519 and Fig. 4, see also Annex A, Fig. A1 e-), where successive segments and breaks corresponding to the Raccah-Vallet's isotherms have been observed.

More recently, **Toroker** and **Carter** examined the possible improving of the conductivity of $Fe_{1-z}O$ by doping the p- or n- conduction mode, with the aim of stabilizing the nanoscale fabrication of wüstite, and then adapting the nanoparticles to create efficient solar light conversion materials [109].

They listed the procedures allowing the calculation of Marcus theory parameters for cluster models with hydrogen dopant and substitutional Cu^+, Li^+ and Na^+. They concluded that « iron vacancies drastically limit the hole conductivity » while Li, H and Na dopants improve it. So, it would be interesting to suppress the formation of vacancies by « alloying FeO », which would amplify the p-type conductivity.

Note: An extensive thermodynamic study of multiple substituted wüstites can be found in the work of Lykasov *et al.* which is reviewed partly in [13] and [111]. Structural aspects of calcio- and magnesio-wüstites are available *infra* (see Table II, and in Fig. 15)).

4.3. Nanocomposites. Epsilon-Fe

Aldon and **Jumas** examine the electrochemical redox phenomena at the negative electrode $Fe/Fe_{1-z_0}O$ formed by wüstite of limit-composition z_0 (= 0.050 ±0.013) in Li-ion batteries [110]. The initial samples of hematite powder, reduced in H_2 at 800 °C, are quenched outside the furnace. The analyses by Mössbauer spectroscopy and X-ray diffraction, after the first discharge, yield the nature and concentration of the products of reduction of wüstite by Li. Nanoparticles of iron (~2nm) embedded in a Li_2O matrix are identified. A part of the iron atoms appearing in the disproportionation is made of the ε-Fe phase which is stressed in the matrix under a pressure evaluated at 6.7 GPa, and which is not ferromagnetic. It can be due to the extrusion from the W structure. At the same time, small clusters of lacunary hematite are formed. These phenomena have been still identified in the formation of « planetary materials, in the Earth's inner core ». See also geological observations by Hazen and Jeanloz [10].

5. Other kinetic and diffusional works

5.1. Iron self-diffusion

In 1963, **Desmarescaux** and **Lacombe** study self-diffusion in using isotopes [55]Fe and [59]Fe [112]. They state experimentally (Fig. 11) that the self-diffusion coefficient D^*_{Fe} increases with z at a given temperature T. At increasing T, because the clusters are dissociated, the rate of free vacancies is increased, the self-diffusion coefficient too. They deduce that self-diffusion proceeded through a vacancy driven mechanism, especially noticeable at high temperature. At lower temperatures, fewer free vacancies and more complex vacancy-electron holes exist. Diffusion is then slower. The number of vacancies associated to Fe^{3+} cations [the clusters] increases with z, so a compensation with the free vacancies implies a quasi-constant D^*_{Fe} whatever z below 850 °C. These observations are interpreted in the Collongues's review [18] with the help of theoretical evaluations of the binding energies in clusters (see Sections *6.5. Cluster stability,* and 6.6. *Diffusion and stability*).
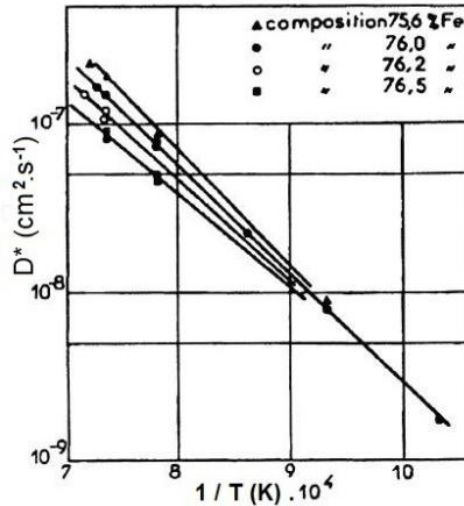
Fig. 11: Fe diffusion (from ref. [112], Fig.4) : log D$^*_{Fe}$ *vs* 1/T.
Fe % = 75.6 ⇔ *z*= 0.112; 76.0 ⇔ 0.093; 76.2 ⇔ 0.083; 76.5 ⇔ 0.067.

5.2. Isothermal kinetics

Landler and **Komarek** measure the loss of mass *vs* time ΔM(t) in H2/H2O mixtures when reducing polycrystalline samples by thermogravimetry [113]. In their calculations, the coefficients of iron self- and chemical diffusion decrease for increasing *z* at constant T∈[800 - 1050 °C] because of « the increased freezing due to repulsive interaction of the vacancies ». That corresponds to activation energy independent of T. This observation is related primarily to the formation of clusters, then to the ordering of clusters in the bulk (see Section *2.7. Trends to ordering*).

Considering the relationship log(ΔM/ΔM$_o$) = n.log t + k, in which ΔM$_o$ is the total mass loss, reduction kinetics data from the authors at 950, 1000 and 1050 °C can be separated into three regimes II, III, and IV (see Annex B, Fig. B1). At 1000 °C, the calculated mean values of n are -0.72 (W3?), -0.49 (W2?) and -0.3 (W1?), respectively [114]. A brief anharmonic sequence is observed at the transitions between two reduction processes. The increase of 0.6 eV in the activation energies E$_{III}$ = 1.31 eV and E$_{II}$ = 1.89 eV, for the reduction sequences III then II, is observed a decreasing *z*, *i.e.*, when the vacancy concentration decreases. It corresponds to the decrease of the ordering on the boundary W3→W2. This variation is opposite to other results in the literature, particularly to ([112] Fig 5, see section *5.1. Self-diffusion*). The three coefficients n are primarily the signature of the bulk modifications by Landler and Komarek, while the three kinetic coefficients m by Worral and Coley are primarily characteristic of surface phenomena [113] [73] (see [115]: Bulk and surface process in the course of the reduction).

Similarly, successive different reduction sequences using H2O/H2 gas mixtures that exhibit transitional anomalies can be observed by **Rieke** and **Bohnenkamp** [116] (see Annex A, Fig. A1 c-).

5.3. In situ diffusion

Rickert and **Weppner** combine a solid galvanic cell for the ionic conduction by O^{2-} through the sample while with the other sample face in contact with a platinum foil [117]. The diffusion is studied *in situ* during the relaxation from a composition to another, driven by controlled impulses of electrical potential. Their main result is that the chemical diffusion coefficient increases with increasing *z* (*i.e.*, with the vacancy concentration), which disagrees with Landler and Komarek [113] and not with any other authors. Transitional anomalies are clearly noticed (see [117] Fig. 6 and 7 p. 1856, and Fig. 8 p. 1857).

6. Relationships between defect structures and the phase diagram

We review key publications from authors who have attempted to solve the key challenge formulated by Carl Wagner in 1930 of linking more tightly defect structure and thermodynamics, such as partial molar properties or the equilibrium constant of formation of the clusters. Kinetics (diffusional) relations were also developed.

6.1. Per Kofstad *and* Zeev Hed

Theses authors remark that z increases at constant p′ as T decreases, which is different than other oxides, and likely due to a complex defect structure [2] [118] (see section *5.1. Iron self-diffusion* by authors [112]). They emphasize that there is some doubt that all the iron vacancies are doubly charged. The electron holes associated to a vacancy can jump into only one of the 12 next nearest octahedral neighbors (Fe_{Fe}°) and one tetrahedral site ($Fe_i^{\circ\circ\circ}$). Most of octahedral vacancies are singly charged.

A model can thus be elaborated from the Roth complex $[V_{Fe}^{m(\prime)} - Fe_i^{n(^\circ)} - V_{Fe}^{p(\prime)}]^{q(\prime)}$, n=1,3, (m,p) = 0,1,2. In the relationship $\sigma \propto p'^{1/S}$, the s value is larger than the value in the similar relationship connecting z to p′ because vacancies would be neutral.

6.2. Toft Sørensen*'s works*

In a book devoted to nonstoichiometric oxides, Toft Sørensen then with El Sayed Ali [9] [46] tentatively identify the defect structure of the « subphases » in using thermogravimetric data [l'- z] at 1000 - 1300 °C exclusively by Bransky and Hed [99]. They consider three main defects (doubly charged vacancy V_{Fe}'', and tetrahedral complex defects $(4:1)^{(m)\cdot}$ and $(6:2)$) as defined by Catlow *et al.* (see [9] chapter 2). They focus on the defect cluster differently ionized, which leads them to define a linear plot of l' *vs* log y ($\equiv z$) with minimal slopes 1/s in the relation $z \propto (p')^{1/s}$. A second criterion concerns the so-called exclusion envelope, *i.e.,* the long-range order as a layer or a close packing structure. They localize in the wüstite equilibrium area T(z) the predominant defect (4:1) plus a layer structure, (4:1) plus a close packing, (6:2) plus a layer structure, according to ΔT layers above 1300 °C, between 1300 and 1200 °C and below 1200°C, respectively. In addition, iron vacancies V_{Fe}'' are present on the right side of a line at composition z close to 0.09 (see [46], Fig. 7 p. 20). So, a structural characterization is roughly proposed, and the phase diagram of Fender and Riley [67] and Vallet and Raccah [44] is approximately drawn again.

6.3. The C(luster) C(omponent) M(ethod)
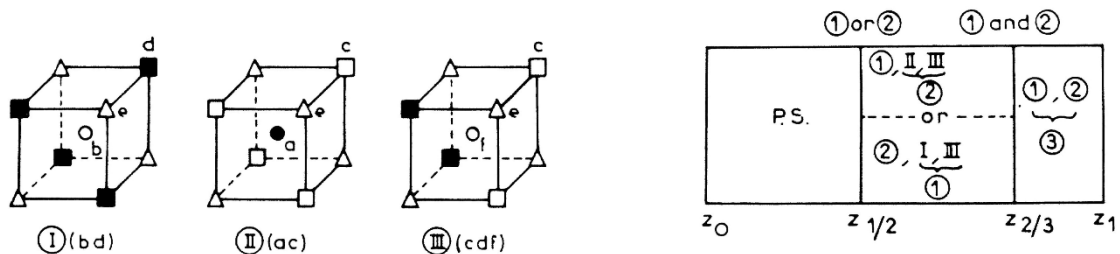
Structural unit blocks S.S. I, II, III: positions ■: (16d), □: (16c), O: (8b), ●: (8a), ⊗: (48f), △: (32e); a and d are for iron, c and f for vacancies (see ref. (6), Table 7.1., p. 186). Short range order in terms of S.S ① and C.C. ① in the three sub-domains; C.C. 1: I-6III, C.C. 2: II-6III, C.C. 3: I-6III-II. In the range [z_o- $z_{1/2}$], II and III increase, I decreases; in [$z_{1/2}$- $z_{2/3}$], II and III decrease, 1 or 2 increases; in [$z_{2/3}$- z_1], 1 and 2 decrease, 3 increases.

Fig. 12: C.C.M. applied to wüstite (from ref. [121]). The three pseudo phases from z_o on the γ-Fe/W1 boundary to z_1 on the W3/Fe3O4 boundary described with the help of three cluster components ①, ②, ③.

In the course of their theoretical work about oxides properties, **Men'** *et al.* were concerned with the wüstite phase [6] [119]. Men' and Carel apply C.C.M. to model the wüstite solid solution [120] [121] [122]. The « cluster components » are defined from crystallographic positions forming unit blocks in the general spinel structure. For example, three cluster components ①, ② and ③, and their concentration as a function of z allow to build the lattice of the wüstite $Fe_{1-z}O$, and to model some of its physical properties, taking into account the pseudo-phases (Fig. 12).

6.4. Other modeling approaches.

Mrowec *et al.* work on defect clustering in the wüstite phase using a collection of data (z, log p′) from the literature [47], [14]. They envisage all the defect clusters suggested by Catlow and Fender [123], *i.e.*, (4:1), (6:2), (8:3), (10:4), (12:4) and (16:5) with several ionization degrees including the highest. Elaborate calculations of the equilibrium constants lead them to the assessment of the enthalpy and entropy of formation of all these ionized clusters, then to $\Delta\bar{H}_O$ independently of z and T, and to $\Delta\bar{S}_O$ for $z \in$ [0.055-0.145]. They conclude that the (4:1) cluster is the most likely to occur and that the ionization degree increases with temperature to reach the maximum value 5- at 1573 K.

Nowotny and **Rekas** [124] describe the defect structure and thermodynamic properties. They investigate the clustering of point defects (iron vacancies and electron holes) across the entire domain using the Debye-Hückel theory, which allows to use a product $\gamma.[x_i]$ in place of $[x_i]$, particularly for $i=h^{\circ}$. With this approach, the activity coefficients are merged with the sole mean coefficient $f_{\pm}$ determined as a function of the ionic force of the solution (and not of its square root). They modeled the interactions during the formation of the cluster (4:1) taking into account activity instead of concentration. Sets of data (z, log p′) and ($\Delta\bar{H}_O$, z) were gathered from the literature. They evaluated the enthalpy and entropy of formation of a cluster $(4:1)^{5-}$ at -396.7 kJ.mol^{-1} and +267.4 J.K^{-1}.mol^{-1}, respectively. They concluded that this cluster $(4:1)^{n-}$ would be the constitutive module of more extended clusters. An expression of the equilibrium constant for the cluster formation is determined across the whole domain independently of the existence of pseudo-phase transitions.

6.5. Cluster stability

Catlow and **Fender** try first to access the defect structure by means of large-scale computation of the binding energies following the Born model [123]. They envisage in a theoretical manner the clusters unity (4:1), edge-sharing (6:2) and (8:3), corner sharing (16:5) precursor of Fe3O4. The location (zone [z, T] of the phase diagram) of these clusters is suggested qualitatively, but not in relation with the pseudo phases.

Later, Catlow *et al.* assessed the formation energy and the relative stability of the clusters by means of the Mott-Littleton method [125]. The cluster (12:4) <110> type by Lebreton and Hobbs is considered as being the most stable extended cluster, after clusters (6:2) and (8:3) [126]. In a summary-paper [127], four classes of clusters are envisaged: corner-sharing clusters (4:1), (7:2), and (16:5); edge-sharing clusters (6:2), (8:3) and (12:4); ZnS blende like cluster (10:4) [127] [128] [129]; clusters (13:4) and (5:2) [130] [131].
The authors note that the (10:4) blende ZnS cluster envisaged by Grimes *et al.* [129] [132] is not the most likely because it was characterized without taking into account the geometric relaxation [127].

Tomlinson and **Catlow** attempt to relate the structural modeling of short-range order, and the macroscopic variation of z as a function of p′. The calculated binding energy per vacancy leads them to order the clusters as follows: [$(8:3)^{+1}$, (12:4), (6:2), $(16:5)^{-1}$, $(12:5)^{-1}$, $(13:4)^{-2}$, $(4:1)^{-1}$, $(10:4)^{-4}$, (5:2 M), (5:2 G)] from 2.24 to 0.71 eV, successively. Finally, they propose a mixture of clusters [(12:4), (6:2), (4:1)] for the incommensurate sub-phase P′ [133].

Then, **Grimes** *et al.* consider the structure and stability of clusters with different coordination types [132] [134]. They base their analysis on a generalized crystal field for the 3d electrons of Fe^{3+} and Fe^{2+}, including the energy of the orbitals 2s and 2p of oxygen. Their computation of the binding energy per

vacancy favors the clusters <110> ZnS blende and <111> spinel type stacking. It rules out clusters (8:3) and (10:4), based on <100> stacking of (4:1) units, and the Koch and Cohen (13:4) cluster. Within the lower field of stoichiometry (P′ phase), smaller clusters coexist including (4:1), (6:2), (7:2) <110>, (10:4) ZnS blende type, and (7:2) <111> spinel type. Larger clusters from the (12:4) <110> type, (18:6), (16:5) spinel <111> type, (16:5) <110> type and (16:7) <110> ZnS blende type clusters can be invoked at higher nonstoichiometry (P″ phase). Finally, they assert that the charge of the clusters should be zero in order to agree with experimental data.

6.6. Diffusion and stability

In a review about nonstoichiometric oxides, **Collongues** [18] envisages particularly the clustering as specified by Desmarescaux and Lacombe (see *section 5.1. Self-diffusion of iron*). The activation energy of the diffusion increases with increasing z, while the opposite effect is the principal rule. « Vacancy clusters » are the reason of this unusual behavior. Catlow *et al.*'s calculations of (Fe^{3+}- vacancy) binding energy indicate that clusters, such as (6:2) or (8:3) of size lower than that of (16:5) (precursor of magnetite), are more stable than this latter cluster. This feature would indicate that even a cluster structurally far from magnetite is responsible of the reduced diffusion process. The existence of three domains in the phase diagram is envisaged.

Note: The classification of the clusters become more complicated because of the increasing number of proposals in the literature. Initially, only the criterion of corner or edge sharing of the basic (4:1) units was needed. Mixed cases were thought to be the exception. Lebreton and Hobbs [126] introduced three way of clustering: *edge sharing along <100> (Type I)*, *corner sharing along <110> (Type II)*, and *corner sharing along <111> (Type III)*. Mixed ways are also to be envisaged. Clusters based on composition alone are possible exceptions (*e.g.*, cluster (10:3)). Labidi and Monty (see [135] p. 100-101) resumed the situation differently with the *types 1 (face shared) aligned in <100> direction, 2 (edge shared) aligned in <110> direction, and 3 (corner shared) aligned in <111> direction*. Worral and Coley (see [22] p. 24-26) classified the clusters in three types defined as either *type 1 (corner shared as in magnetite)*, *type 2 (edge shared sharing one octahedral vacancy)*, or *type 3 (edge shared sharing two octahedral vacancies)*.

## 7. Structural approaches. Models for short- and long-range ordering

7.1. Roth *model: the cluster* (2:1)

Considering the experimental uncertainties inherent to X-ray diffraction on polycrystalline oxides, it is more suitable to use neutron diffraction experiments to determine correctly the site occupancies relative to iron atoms in octahedral and tetrahedral sites of the NaCl-like lattice. Initial results relative to quenched wüstite are obtained using neutron diffraction by **W. L. Roth** who determines the octahedral and tetrahedral site occupancies of vacancies and Fe^{3+} cations, respectively represented by ($z+t$) and t [35]. The characterization of the ratio R = ($z+t$)/t was found close to R=2 for samples quenched from high temperatures. The neutron diffraction patterns obtained at 290 K and 4.2 K suggested the presence of defects constituted of two cation vacancies associated with one interstitial cation in the tetrahedral site. These two characteristics suggested a trend to the magnetite structure. In addition, the average magnetic moment per cation site was found to be much smaller than expected.

7.2. The historical Koch and Cohen cluster (13:4)

In 1969, **Koch** and **Cohen** publish a study by X-ray diffraction on a single crystal of wüstite $Fe_{0.902}O$ (z=0.098) obtained after quenching from 1000 °C, and « corresponding to the P′ phase of Manenc » [130].

The authors proposed a new commensurate defect structure based on (13:4) large clusters (Fig. 13) distributed in the fcc lattice (cell parameter a) with a repetition distance (3a, 3a, 3a) noted as 3X. For the first time, a detailed crystallographic determination proposed a cluster corresponding to the corner sharing <110> type agglomeration of four basic (4:1) clusters.
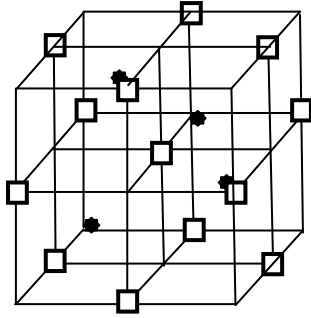
Fig. 13: The Koch and Cohen cluster (13:4) associated with a 3X commensurate structure of wüstite $Fe_{0.902}O$.

To perform their structural refinements, the authors fixed this cluster model assuming that the resulting superstructure should have a periodicity of 3X (the clusters being arranged only with regular distances of three cell parameters), in agreement with the known composition z=0.098, despite the fact that the additional peaks correspond to a superstructure 2.6X incompatible with their assumption.

7.3. Neutron diffraction

Using *in situ* neutron diffraction experiments, **Cheetham, Fender** and **Taylor** [136] show that the ratio R = $(z+t)/t$ ranges between 3 and 4, with a mean value of 3.2, which can be compatible with a specific (13:4) cluster (R = 3.25).

Using neutron diffraction at low and room temperature, coupled with magnetic scattering, **Battle and Cheetham** determine ratios R = 2.78, 2.82, and 3.01 and conclude that a cluster (8:3) can be consistent with their observations [137] and the preceding calculations of Catlow *et al.* (see [9] Chapter 8 p. 407-410: summary of these results by Cheetham). They couple neutron diffraction experiments to Mössbauer effect analyses and study the antiferromagnetic coupling of iron cations in octahedral and tetrahedral sites of the FeO lattice (see [137] Fig. 4 p. 343). For the first time, these authors show that atomic clustering observed in quenched samples (out of equilibrium) can be characterized from the study of magnetic properties of clusters in a lattice. This result will be used again by Saines *et al.* [138].

The numerous results obtained by **Radler, Cohen** and **Faber jr** from neutron diffraction patterns of polycrystalline samples, under equilibrium, yield values of R > 3 corresponding to mixtures of clusters at high temperature, and R < 3 to clusters larger than (10:3) below 1173 K [139]. This result could indicate a possible differentiation between the structures of W and W'.

Schweika *et al.* find a ratio of vacancies to interstitials R = 4.0 (±0.5) obtained under *in situ* conditions by neutron diffuse scattering from a single crystal with composition z = 0.08, at T=1150 °C [140, 141]. Their analysis of the diffuse scattering patterns leads them to conclude that 30% of the vacancies are free, while a further 15% of the defects are bound in isolated clusters (4:1). In their analysis, the authors state that their results invalidate the predominance of large clusters at elevated z. For example, the (13:4) cluster cannot fit the diffuse scattering that they characterized near the origin.

Saines *et al.* in Cheetham's team study by neutron diffraction a polycrystalline sample of wüstite $Fe_{0.902}O$ quenched from 900 °C (from the domain of W') [138]. They derive nuclear and magnetic clusters from an elaborate Reverse Monte Carlo modeling technique. The nuclear structure is described by islands of V4T units connected along the <110> directions « into a Koch-Cohen arrangement ». The magnetic structure in the bulk between the clusters is described as a « non-collinear variant » of the antiferromagnetic structure along the [111] axis as previously envisaged in [137]. Free vacancies are near the clusters. This structural approach can be compared with the paracrystalline description of the defect distribution by Welberry *et al.* [142] [143] [144].

7.4. X-ray diffraction

Welberry *et al.* present a detailed study of X-ray diffuse scattering for a single crystal with composition z=0.057, obtained after quenching from a temperature which is not specified. Their sample corresponds either to the Manenc's phase P (see [75] [76]), or to the W1 domain proposed by Vallet *et al.* [26]-[29]. The X-ray diffuse scattering analysis coupled with a paracrystalline modeling gives information on defect distribution, defect cluster size, number of interstitials, and lattice strain. The authors describe (statistically) a specific crystal constituted of ordered zones of clusters randomly distributed in a fcc lattice [142] [143] [144].

7.5. Gavarri *et alii 's* works

In 1979, using *in situ* neutron diffraction experiments, Gavarri, Carel and **Weigel** develop an analysis of the structural evolution of wüstite in CO2/CO environments at high temperature [145]. A systematic determination of the ratio of the vacancy rate $(z+t)$ divided by the interstitial rate t, R= $(z+t)/t$, is carried out. Quasi constant values of R close to 2.4 ± 0.4, at two equilibrium temperatures (985 and 1075 °C) and compositions z ranging between 0.058 and 0.120, are determined, with standard errors induced by the uncertainties on the separation between Bragg peaks and a complex diffuse scattering.
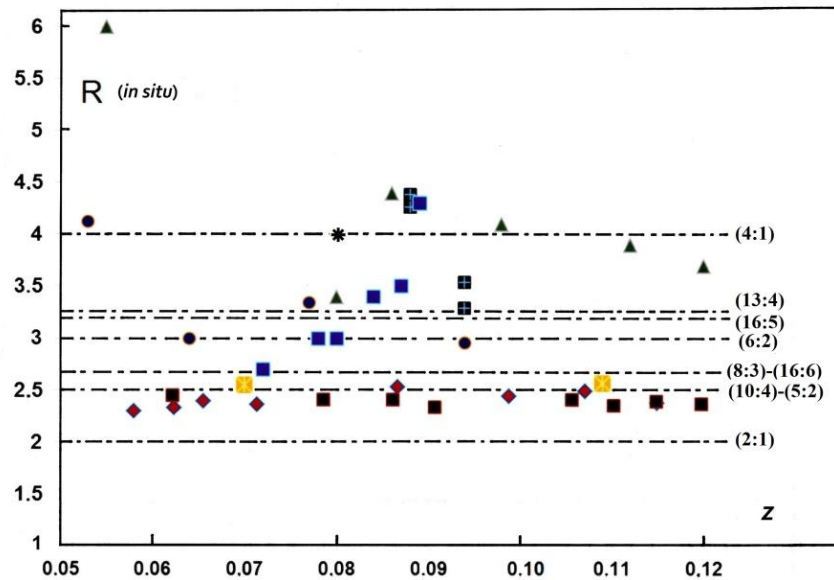
Fig. 14: R =$(z+t)/t$ values *vs z*, determined under equilibrium, from the literature.
■: at 900°C [131]; ●: at 800°C and ✚ : at 925, 1050, 1125, 1180°C [136]; ▲: at 1050°C and ■ : at 850-1100°C [139]; ✳: at 1150°C [141]; ◆ : at 1075°C and ■: at 985°C [145].

Fig. 14 displays the values of R obtained by different authors. In the case of studies made *in situ*, most of the values of R range between 2.4 and 3.5. The authors observe two types of signals: (i) Bragg peaks from which the ratio R is determined, (ii) additional scattering corresponding to superstructure peaks, and thermal and static diffuse scattering associated with defect clustering, disorder and static distortions (see [145] and *infra* Fig. 15). The intensities $I_A(T, z)$ of this additional scattering increases linearly with composition z and decreases with temperature.

The ratios I_A/I_{220}, where I_{220} is the intensity of the (220) Bragg peak, vary as follows:

- $\quad I_A/I_{220}$ (985 °C) $= 0.19 + 4.05(z\text{-}0.062)$ \hfill (23)

- $\quad I_A/I_{220}$ (1075 °C) $= 0.15 + 4.25\ (z\text{-}0.058)$ \hfill (24)

Therefore, these linear variations coupled with a small variation of the superstructure parameter k suggest a quasi-invariance of cluster size with clusters agglomerated in domains, and with the size of these domains

increasing with z. The position of the centroid of this scattering allows the determination of an average superstructure corresponding to an irregular spacing of clusters quasi-constant with z or T. The average distance between clusters is evaluated to $2.7a_0$, a_0 being the cell parameter of ideal wüstite for a fixed temperature.

In later works by neutron diffraction on quenched samples of magnesio- and calcio-wüstites, using Rietveld refinements, Gavarri *et al.* [128] [146] determined R values close to 2.5 for pure wüstites or for magnesio-wüstites $Fe_{(1-z-y)}Mg_yO$. In the case of calcio-wüstites $Fe_{(1-z-y)}Ca_yO$, as the composition y increased, the ratio R increased strongly with R > 4 and the superstructure vanished. Under these conditions, the cluster sizes would be strongly modified, and a majority of free vacancies would appear likely. These studies demonstrate that the formation of clusters is stabilized by Mg doping, and destabilized by Ca doping, producing free vacancies coexisting with residual clusters.

Fig. 15 shows a neutron diffraction pattern obtained from a quenched polycrystalline calcio-wüstite ($z= 0.065$; $y = 0.030$; R = 3.3 ±0.5). In addition to Bragg peaks, the complex signal due to the superstructure and the structural disorder can be observed.
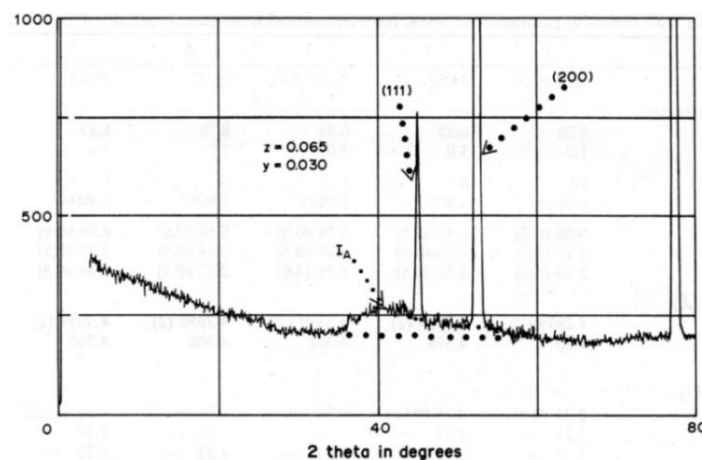

Fig. 15. Neutron diffraction pattern (λ = 1.9 Å) of a quenched polycrystalline calcio-wustite $Fe_{1-z-y}Ca_yO$ in room conditions [146]. Presence of a large diffuse scattering (I_A) due to the superstructure (k close to 2.7), and (110) small peak (36° 2θ) due to vacancies and interstitial Fe^{3+} in the lattice. The intensity of I_A decreases with the calcium fraction y. Cell parameter a(25 °C) = 4.3164 Å. R=(z+t)/t=3.3.
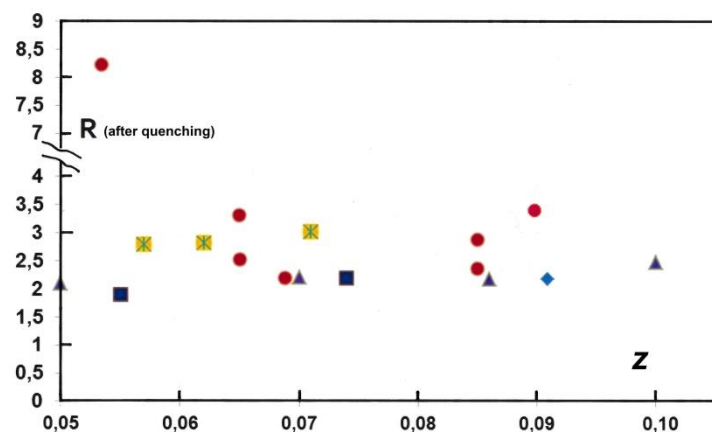

Fig. 16. R values *vs z* from literature determined after quenching.
Quenched $Fe_{1-z}O$: ◆ : Gavarri, Carel, Weigel [145];
WMg and WCa: ● : Carel and Gavarri [146];
Quenched $Fe_{1-z}O$: ■ : Roth [35]; ▲ : Smuts [147]; ✳ : Battle and Cheetham [137]

It is to be noted that the diffuse scattering due to long-range ordering is similar in diffraction patterns of quenched and *in situ* samples. Consequently, only a slight difference would exist between high temperatures and room temperature for the nature of defects and their organization in the fcc lattice.

Table 2 lists the values of R corresponding to the quenched pure and substituted wüstites resulting from these studies (magnesio- and calcio- wüstites are noted WMg and WCa respectively). The values of the ratio R = $(z+t)/t$ obtained from the literature on quenched, pure and Ca or Mg substituted, wüstites are displayed in Fig. 16. The utmost value R = 8.2 is obtained for a calcium rich calcio-wüstite (y=0.05).

Table 2- R = $(z+t)/t$ values obtained from Rietveld analyses
**of neutron diffraction patterns of quenched substituted wüstites (from ref. [146]).**

$Fe_{1-z-y} Mg_y O$	Fraction y (Mg)	R = (z+t)/t (*)
z=0.065	0.075	2.53(0.5)
z=0.085	0.030	2.88(0.6)
$Fe_{1-z-y} Ca_y O$	Fraction y (Ca)	R = (z+t)/t
z=0.0688	0.010	2.20(0.5)
z=0.0649 (**)	0.030 (*)	3.31(0.5)
z= 0.0534	0.050	8.22(4.0)
z=0.085	0.010	2.37(0.5)
z=0.0899	0.030	3.39(0.5)

(*) experimental uncertainty (due to diffuse scattering); (**) See Fig. 1**6**.

7. 6. T(ransmission) E(lectron) M(icroscopy) analyses

In the past, microstructural analyses using electron diffraction and HREM images were performed (see **Andersson** and **Sletnes** [76]). The images obtained by **Iijima** for a sample $Fe_{0.92}O$ « *provided by Prof. Cohen* » are often referenced [79]. The presence of the hypothetical cluster (10:4) <110> type with a ZnS-blende configuration has been particularly envisaged.

When re-interpreting the images obtained from electron microscopy experiments by Ishiguro and Nagakura [148], Gavarri, Carel, Weigel [149], then **Nihoul**, Gavarri, Carel [150] show that this cluster corresponding to the ideal ratio R = 2.5 is compatible with the experimental data available (at least for quenched wüstites). This cluster depicted in Fig. 17 is formed of a « FeO » cubic cell surrounded by an envelope of Fe^{3+} cations with total 3D dimension (2a x 2a x 2a).
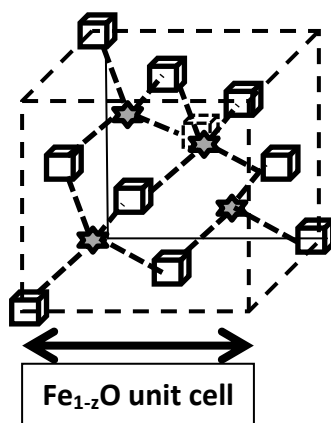
Fig. 17. The cluster (10:4) ZnS blende <110> type.

✿ = **Fe^{3+} in tetrahedral site**

⬚ = **Iron vacancy in octahedral site**

$Fe_{1-z}O$ unit cell

In the case of crystals quenched from 1000 °C, and with a composition $z = 0.10$ [148], the formation of local ordered domains of these clusters can be at the origin of all observations corresponding to a mean ratio R close to 2.5, and a quasi-invariant superstructure. The authors propose a progressive ordering of clusters as z increased: for low z values, repetition distances 3a linkable to variety P by Manenc [73], or W1, are observed. For intermediate z values, repetition distances 3a and (2.55a x 2.55a x 2.55a) are formed in local zones linkable to W3 or P″.

A specific well-ordered superstructure can be based on a 3D supercell with parameters (5a x 5a x 5a). This superlattice can be associated with the limit evolution at the boundary W3/Fe3O4. Such a superstructure was depicted at equilibrium by Shaïovitch, Zvinchuk and Vergazov [91]. Finally, the distinction between « varieties of wüstite » or pseudo-phases can be due to both modifications of long-range order of clusters and the coexistence of different clusters that include free vacancies.

To define an isolated cluster correctly, particularly the ZnS blende defect cluster (10:4), it is necessary to take into account its envelope of Fe^{2+} and Fe^{3+} cations in octahedral sites.

The charge of the cluster can be postulated as a first approximation by assuming the individual charges of vacancies and of iron atoms. In Fig. 18 is illustrated the possible arrangement of these defect clusters (10:4), in the fcc lattice. The minimum distance between clusters is $[(2.5a)^2 + (0.5a)^2]^{1/2} = 2.55a$, and with allowed distances up to 3a. This model is based on a cluster core (10:4) with double envelope of octahedral iron cations.

If we assume that a cluster (m:n) has a global charge Q= 3n-mq (m vacancies with formal charges q (=2,1,0) and n interstitials $Fe_i^{\circ\circ\circ}$ with charges +3), then the (10:4) cluster has a charge of Q= -8, +2, or +12 for q= 2, 1 or 0, respectively. The electroneutrality is ensured by envelopes with charges -Q.

Using this type of defect structure, a model of ordered (10:4) clusters is proposed [149] [150], thus allowing simulation of HREM images in the two directions [001] and [101] of the crystal. These hypothetical distributions of clusters (Fig. 19) are in agreement with the HREM images by Ishiguro and Nagakura [148].
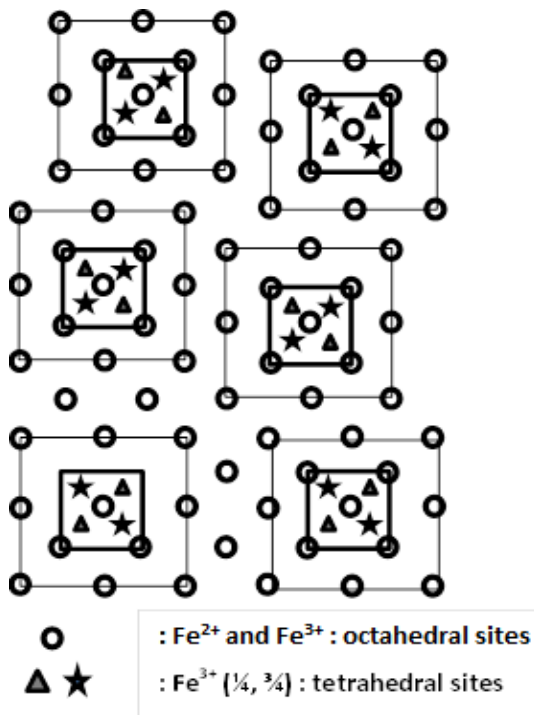

Fig. 18. Various orderings of clusters (10:4) in the fcc lattice of wüstite. The basic cluster can be the (13:4), the (10:4) or other possibilities with 4 interstitial sites occupied by cations Fe^{3+}. The disorder can develop by statistical displacement in one, two or three directions. 2.55a could be the smaller inter-cluster distance (a = cell parameter of the "FeO" lattice).

○ : Fe^{2+} and Fe^{3+} : octahedral sites

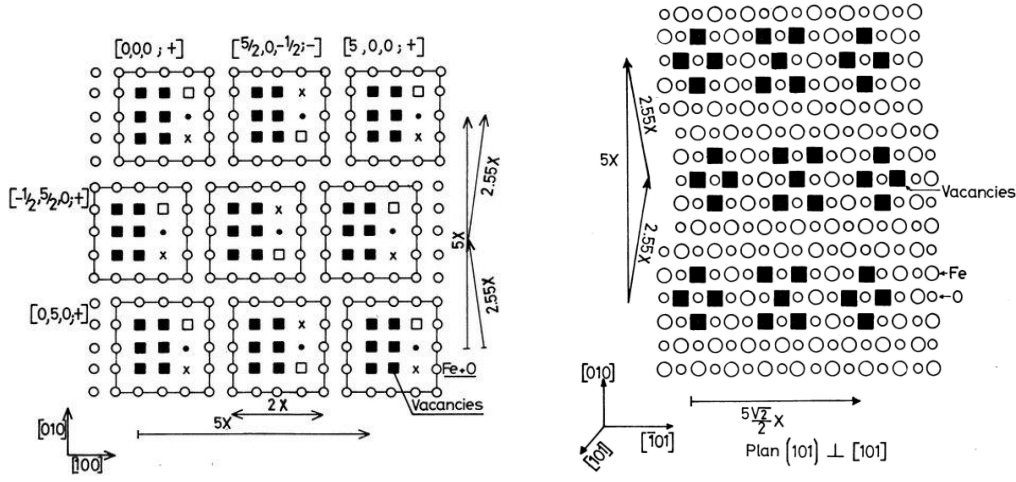△ ★ : Fe^{3+} (¼, ¾) : tetrahedral sites

Fig. 19. Model of local ordering of (10:4) blende ZnS clusters, in agreement with the experimental HREM images by Ishiguro and Nagakura [148] (from ref. [149]).

8. Hypothesis of a mixture of defect clusters, and/or cluster zones

8.1. *Mixture of clusters*

Based on previous publications by Gavarri *et al.* [145] [151], a specific relationship can be established taking into account ordered zones of clusters and zones in which free vacancies are distributed. A mixture of different clusters $(m:n)_1$ and $(m:n)_2$ can coexist with additional free vacancies. As a first approximation, the authors consider a lattice based on N cells of $Fe_{1-z}O$, with a proportion $V(z)$ of zones without defect. If N_i is the number of cells where clusters $(m:n)_i$ are formed, with the characteristics m_i and n_i of a specific cluster, and the distance $k_i.a$ between two clusters, then the relation between cluster size and long-range order in the case of the fcc lattice of wüstite can be expressed as follows:

$$1-V(z) = 4z . \Sigma_i \{ \pi_i (k_i)^3 / (m_i-n_i) \} \text{ with } \pi_i = N_i/N \qquad (25)$$

For a unique cluster with continuous order (high z values), the relation (25) yields:

$$(m-n) / (k)^3 = 4z \quad \Rightarrow \quad (m-n) = 4zk^3 \qquad (26)$$

Considering the experimental values of k available in the literature, ranging between 2.5 and 3, this parameter k is characteristic of zones in which clusters are ordered partially. This means that, for low values of z, zones without clusters would exist and that they would be occupied by isolated defects (*i.e.*, free vacancies). The major part of the crystal lattice would be dominated by disordered point defects, and electrical conduction would be due to holes. For intermediate values of z, the cluster zones would be progressively joining together, forming percolation paths of ordered zones. A mixed conduction mode would be expected. For high values of z, the lattice would be occupied fully by ordered clusters, with likely small changes in the arrangement of clusters. Electrons in conduction band would mainly condition the electrical conduction.

This hypothetical description is in correspondence with the W1 disordered pseudo-phase and a conduction of p type, the intermediate pseudo-phase W2 as a mixture of cluster zones and free vacancy zones with mixed conduction, *i.e.*, (holes +) and (electrons -) coexisting at short distance, and the ordered pseudo-phase W3 with conduction of n type from electrons in the conduction band.

8.2. Variation of parameter k

Numerous structural data can be found in the studies by **Bauer, Pianelli** *et al.* ([8] Part I and [152] Part II). These authors develop a series of experiments using X-ray diffraction on powders of quenched wüstites. They observe linear variations of the cell parameter as a function of composition z, and of the position of superstructure peaks. They characterize these peaks with parameter $\delta = 1/k$, where k designates the superstructure parameter discussed previously. Parameter δ varies between 0.37 and 0.39, corresponding to values of k between 2.7 and 2.56. This variation observed in quenched samples is in good agreement with the model presented in (section *7.6. TEM analysis*) with a minimum k value of 2.55. Authors [8, 152] consider that their data did not permit to observe any phase transition. However, they suggest that wüstite can be described by an incommensurate lattice of clusters, with the presence of different clusters based on cluster (4:1).

8.3. Statistical analysis of diffuse scattering

Gartstein and Mason [106] show that p conduction is observed in wüstite and that electrical conduction is based on a hopping mechanism between adjacent clusters. Later, Gartstein *et al.* publish a crystallographic analysis of a $Fe_{1-z}O$ (z=0.07) single crystal using X-ray diffraction at 1173 K [131] and [153]. They develop a detailed analysis of diffuse scattering and Bragg peaks, and conclude to the existence of a mixture of clusters (13:4) and asymmetric new clusters (5:2) constituted of 5 vacancies and 2 interstitials corresponding to the ideal ratio R = 2.5. They propose an ordering of these clusters with an average repetition distance of 2.5a, close to the hypothetic value of 2.55a proposed in [149] [150].

8.4. Summary

To conclude this section, it can be noted that there is an inherent difference between the concept of a mixture of disordered clusters with various forms, and the concept of zones with identical disordered clusters, coexisting with zones of free point defects. The concept of incommensurability, applied to specific compositions z, was also proposed as a mathematical approach of disorder (see Yamamoto [154] and Weigel *et al.* [155]). Finally, the proposition of the irregular cluster (5:2), resulting from the analysis of diffuse scattering by Gartstein, Mason, Cohen [131] [153], seemed to be compatible with the quasi-constant value $R=(z+t)/t = 2.4 \pm 0.4$ [145].

9. Defect clustering and equilibrium equations

In this section, using basic equilibrium equations from the literature (see particularly [9] and [46]), we propose a new presentation of defect equilibrium equations for wüstite.

It is important to remind that, in $Fe_{1-z}O$ where only Fe^{2+} (also noted Fe_{Fe}) and Fe^{3+} cations (also noted $Fe_{Fe}^{°}$ or $Fe_{Fe}^{°°°}$, for cations in octahedral or tetrahedral sites, respectively) can coexist, cation vacancies can have one of three possible stable charges: doubly charged vacancies V_{Fe}'', simply charged vacancies V_{Fe}', and neutral vacancies V_{Fe}^{x} (noted V_{Fe}). Singly charged iron vacancies V_{Fe}' were proposed previously in place of doubly charged vacancies V_{Fe}'' by Kofstad and Hed [118]. Vacancies of the oxygen sublattice are not considered because they occur in negligible numbers compared to the iron vacancies.

In section *2.2. Modifications or pseudo-phases,* the equilibrium constant (4b) of the hypothetical equilibria (4a), in which the activity of oxygen O_O in the solid is taken equal to 1, can be developed with q=0, 1 or 2 following the general expression in which s =2(q+1):
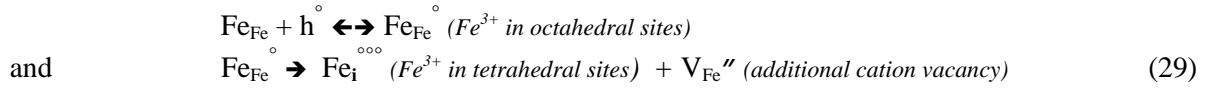
$$\log z = (1/s). \, l' + (1/s) \log (K/C)^2 \quad (\text{with } C = (q)^{2q}) \qquad (27)$$

(identical to equation (4c)). The three hypothetical values of s corresponding to q = 2, 1, and 0 are s = 6, 4, and 2, respectively.

The modifications of q can be described in terms of two equilibriums involving holes $h^{°}$ in the valence band

$$V_{Fe}'' + h^{°} \leftrightarrow V_{Fe}' \qquad \text{and} \qquad V_{Fe}' + h^{°} \leftrightarrow V_{Fe} \qquad (28)$$
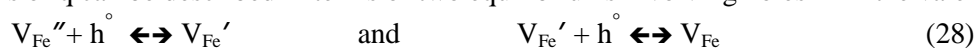
Therefore, three domains corresponding to the three types of iron vacancies can exist in all systems presenting significant cation deficiency. In the case of $Fe_{1-z}O$, additional reactions occur since two valences (Fe^{2+} and Fe^{3+}) exist:

$$Fe_{Fe} + h^{°} \leftrightarrow Fe_{Fe}^{°} \quad \textit{(Fe}^{3+}\textit{ in octahedral sites)}$$

and $\quad Fe_{Fe}^{°} \rightarrow Fe_{i}^{°°°} \quad \textit{(Fe}^{3+}\textit{ in tetrahedral sites)} + V_{Fe}'' \textit{ (additional cation vacancy)} \qquad (29)$

As a first approximation, assuming that the sole point defects are iron vacancies, associated with Fe^{3+} ($Fe_{Fe}^{°}$) and coexisting with Fe^{2+} (Fe_{Fe}) in $Fe_{1-z}O$, the general relationship between composition z and oxygen partial pressure p' is as follows

$$q\, Fe_{Fe} + \tfrac{1}{2} O_2 \leftrightarrow q\, Fe_{Fe}^{°} + V^{q(\prime)} + O_O \quad \rightarrow \quad K_q = [Fe_{Fe}^{°}]^{q}.[\, V^{q(\prime)}] / ([Fe_{Fe}]^{q}.p'^{\frac{1}{2}}) \qquad (30)$$
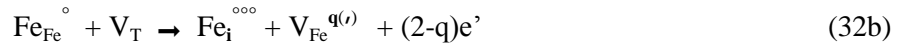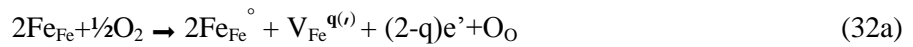
In this expression, $[Fe_{Fe}] \approx 1-3z$ and $[Fe_{Fe}^{°}] \approx 2z$.
As all molar fractions are related to the composition z, the next relation can be derived:

$$K_q = [Fe_{Fe}^{°}]^{q}.[\, V^{q(\prime)}] / ([Fe_{Fe}]^{q}.p'^{\frac{1}{2}}) = 2^{q}.z^{(q+1)}/(1-3z)^{q}.p'^{\frac{1}{2}} \qquad (31)$$

If this simple model is correct, then the term $(1-3z)$ should vary slowly with z in a reduced composition range, meaning that the activity of Fe_{Fe} can be considered as being constant. Under this assumption, z is roughly proportional to $(p')^{1/S}$, with $s = 2(q+1)$ being an integer characteristic of the nature of the defects. For $q = 2$ (doubly charged vacancies) we obtain $s \approx 6$. For $q = 1$ (singly charged vacancies), $s \approx 4$. For neutral vacancies, $s \approx 2$.

Now, let us consider complex clusters $(m:n)^Q$ with variable formal charge Q and successive reactions in which vacant tetrahedral sites V_T are introduced:
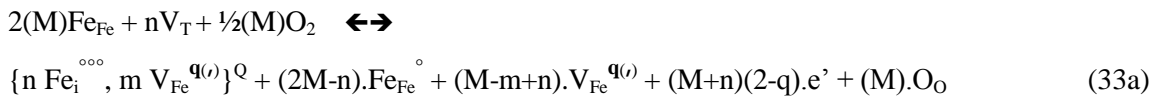
$$2Fe_{Fe} + \tfrac{1}{2}O_2 \rightarrow 2Fe_{Fe}^{°} + V_{Fe}^{q(\prime)} + (2-q)e' + O_O \qquad (32a)$$

$$Fe_{Fe}^{°} + V_T \rightarrow Fe_{i}^{°°°} + V_{Fe}^{q(\prime)} + (2-q)e' \qquad (32b)$$

The formation of stable cluster can be written:

$$nFe_{i}^{°°°} + mV_{Fe}^{q(\prime)} \rightarrow \{n\, Fe_{i}^{°°°}, m\, V_{Fe}^{q(\prime)}\}^Q \qquad (32c)$$
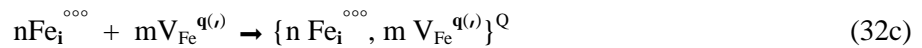
with $Q = 3n-qm$ (positive or negative charge). The cluster will be noted: $CL = \{n\, Fe_{i}^{°°°}, m\, V_{Fe}^{q(\prime)}\}^Q$.
The formal charge Q of a cluster is assumed to result from individual charges of vacancies with the invariant charge of interstitials Fe^{3+} ($Fe_{i}^{°°°}$) as a first approximation. However, the Fe^{3+} interstitial can be modified into Fe^{2+} interstitial cation due to electron jumping, and as a result a more complete model should take into account various possible Q values of cluster charges due to the modification of interstitial cation charges.

Considering the formation of clusters CL coexisting with point defects $Fe_{Fe}^{°}$ and $V_{Fe}^{q(\prime)}$, a more elaborate equation (32a) can be expressed as follows:

$$2(M)Fe_{Fe} + nV_T + \tfrac{1}{2}(M)O_2 \leftrightarrow$$

$$\{n\, Fe_{i}^{°°°}, m\, V_{Fe}^{q(\prime)}\}^Q + (2M-n).Fe_{Fe}^{°} + (M-m+n).V_{Fe}^{q(\prime)} + (M+n)(2-q).e' + (M).O_O \qquad (33a)$$

with the hypothesis: $Q = 3n-qm$ (positive or negative).
In equation (33a), the integer $M \geq m$ is introduced arbitrarily to take into account the possible presence of additional free species $Fe_{Fe}^{°}$ and $V_{Fe}^{q(\prime)}$, associated with free electrons in the conduction band. The additional vacant tetrahedral sites are the vacant sites V_T able to receive an interstitial cation $\underline{Fe_{i}^{°}}$.
As a major fraction of these sites (8 sites for 4 FeO units in a fcc cell) is vacant, their activity can be considered as being quasi-constant, and does not play a significant role in the calculation of equilibrium

constants. The resulting equilibrium constant is as follows, with the reduced notation $[CL] = [\{n\ Fe_i^{°°°},\ m$ $V_{Fe}^{q(\prime)}\}^Q]$:

$$K(T) = [CL].[Fe_{Fe}^{°}]^{(2M-n)}.[V_{Fe}^{q(\prime)}]^{(M-m+n)}.[e']^{(M+n)(2-q)} / ([Fe_{Fe}]^{2M}.[V_T]^n.(p')^{M/2}) \qquad (33b)$$

In this expression, the cluster concentration [CL] is considered as being proportional to z, at least as a first approximation. Applying the same approximation as in previous equilibrium equations, the equilibrium constant can be expressed as follows:

$$K(T) = z.z^{(2M-n)}.z^n.z^{(M+n)(2-q)} / ((1-3z)^{2M}.(p')^{M/2}) \quad \approx \quad z^{(2m+1+(2-q)(m+n))} / (1-3z)^{2m}.(p')^{m/2} \qquad (33c)$$

No activity coefficient is taken into consideration. Consequently, in a restricted range of composition z, no significant change of interactions occurs between point defects or clusters. To illustrate the possible values of parameter s corresponding to the three hypothetical q values, l' has been simulated as a function of log z using the expressions of K(T). The slopes of the curves (l' *vs* log z) were determined. The two specific clusters (4:1) and (10:4) have been chosen to calculate the various coefficients s depending on the charges q of vacancies.

The results are:
- for a cluster (4:1), the three coefficients s are equal to 5.7, 8.2 and 10.7 for q=2, 1 and 0, respectively;
- for a cluster (10:4), the three coefficients s are equal to 5.4, 8.2 and 11 for q=2,1 and 0, respectively.

It can be noted that, for either the cluster (4:1) or the cluster (10:4), the coefficients s resulting from the calculations are quite similar for a given value of q. Given the approximations included in the model and expected experimental uncertainties, these simulated values (from s = 5 to 11) can be considered as being congruent with the experimental s values obtained in the literature and ranging between 4 and 10. In other terms, the existence of pseudo-phases might be reasonably thought to be associated with the variation of the electrical charges (q-) of cation vacancies, and, more generally, with the variation of the electrical charges Q of the clusters.

These changes of electrical charges are strongly correlated with the increasing density of them: in other terms, two neighboring vacancies V″ with the same negative charge 2- can produce two singly charged V′ or neutral V^x vacancies, which will decrease the coulomb repulsion between them, and require additional free electrons migrating in the conduction band.

Now, using this general approach delivering specific s values, it is possible to justify the various modifications observed by many authors including Vallet *et al.* [26-27, 29], Geiger Levin and Wagner [65], Fender and Riley [67], Takayama and Kimizuka [70], Worral and Coley [73]. In particular, let us recall the values s(W1) = 4.6, s(W2) = 6.2, s(W3) = 9.2, extracted from the data by Vallet *et al.* , as well as values s(W1) = 4.8, s(W2) = 6, s(W3) = 9 extracted from the data by [70] (see section *3.7. Takayama and Kimizuka's phase modifications*).

Considering the set of values s = 4.6, 6, 9 associated with W1, W2 and W3 respectively, for low values of z, the existence of doubly charged iron vacancies $V_{Fe}″$ can be associated with a major population of holes corresponding to mode 'p' of conduction. For high values of z, the existence of singly charged or neutral vacancies can be associated with mode 'n' of conduction, *i.e.*, to the injection of electrons in the conduction band. For intermediate values of z, an intermediate state would exist with a mix of holes in the valence band and electrons in the conduction band, following a rate varying from $z_{1/2}$ to $z_{2/3}$.

These considerations can be supported by the p-n transition [89] described many times in the literature (see Fig. 10). The authors provide a detailed interpretation for the existence of various defect configurations corresponding to pseudo-phases in the entire wüstite phase diagram.

For mean values of z, neutron diffraction data show that the clusters are assembled in limited ordered zones. For high values of z, the ordered cluster zones percolate (see [90] HREM images for $z=0.08$ and

z=0.10). The change in vacancy charge as z increases can be accompanied by injection of free electrons in the conduction band. As temperature T increases, the size of the cluster zones decreases, and the number of cluster zones increases. Correlatively, the population of free defects increases.

Taking into account all these considerations, the W1 pseudo-phase can be associated with a small number of clusters assembled in cluster zones, and a large population of free defects with numerous free V_{Fe}'' vacancies. In this domain, holes can be the major electric charge carriers. The W3 pseudo-phase is constituted of large cluster zones, covering the entire lattice adjacent to the magnetite zone. The neutralization of vacancies (or decreasing q charges) shall be associated with a large number of electrons occupying the conduction band. As the W2 pseudo-phase was previously considered as a mix system of pseudo-phases W1 and W3 by several authors, properties can be expected to follow continuous evolutions. In other terms, an intermediate structural configuration can exist, corresponding to the formation of percolation paths allowing a mix conduction of holes and electrons.

10. Percolation approach

A primitive « composite picture » of a possible evolution of the defect structure needing only two clusters and distinct populations through the subdomains was proposed earlier [156]. Nearly at the same time, a similar simple model of the defect structure was proposed in terms of the so-called theoretical Cluster Component Method (see Section 6.3. *The C. C. M.,* Fig. 12).

In Fig. 20, a representation of the distribution of cluster zones (CLZ) inside the lattice is drawn as a schematic percolation process. The size of cluster zones (CLZ) (represented by black squares) is conditioned by the equilibrium temperature. White squares represent zones with only disordered point defects (free vacancies, individual Fe^{3+} in octahedral or tetrahedral sites).

- In the W1 domain, the CLZ's are isolated and immersed in a defect lattice. The transition line W1/W2 corresponds to a specific threshold $z_{1/2}$ value (for fixed T) where there is a starting percolation state.
- The W2 domain might be constituted of large black zones, with percolative paths through the lattice or both types of zones. The W2/W3 transition line might be reached when the residual white zones are no more percolative.
- The W3 state is reached when black zones envelop white zones up to a limit state where all the lattice is covered by a continuum of clusters, *i.e.*, at the boundary W3/Fe_3O_4.

The effect of temperature is to modify the sizes of clusters zones and the limits of composition for each boundary. As temperature increases, the cluster zones are destabilized, and the size of these zones decreases.

Because of the complexity of the system, it is obvious that no unique specific model can represent the various evolutions. Nevertheless, this approach shows that the modifications W1, W2, W3 may be justified simply from changes in electrical charges of point defects, so of clusters, and are strongly correlated with composition z, and the degree of ordering. This scheme implies nearly continuous transformations from Wi to W(i+1) at the level of the slight deviations from the main diffraction process. However, the discontinuities observed in the partial molar properties (see *supra* Fig. 6 and 7), and in the kinetic reduction rates by [73] at the compositions $x_{i/j}$ of the boundary of the subdomains correspond to abrupt and small-scale differences in internal energy and configurational entropy, due to the change of cluster type (or charge), and to the change in long range order of the clusters (see also [113] [114] in Fig. B1 of Annex B).

Note: Metastabilities encountered in most of the experimental studies can modify the location of the transitions i⇄j, *i.e.*, the characteristic $z_{i/j}$ values as determined by thermodynamic assessments, even suppressed them. As examples, the thermogravimetric isotherms (W area) in Raccah's study [40] are grouped together considering a sole modification in certain temperature intervals, without break all along from γ-Fe/Wi to Wi/Fe3O4: W3 at 920, 950, 1000°C, W2 at 1067, 1122, 1140 °C, W1 at 1160, 1167,1200, 1250 °C.
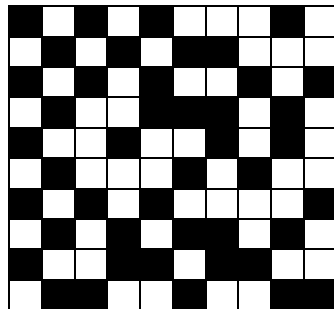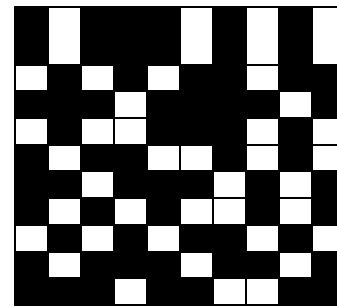
1-Low z values: pseudo-phase W1
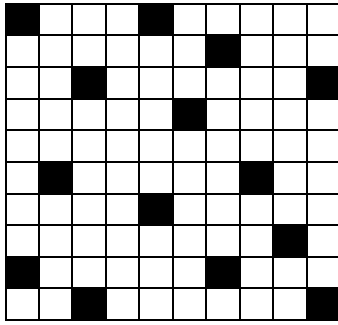
2-Start of percolation: threshold $z_{1/2}$ value on the boundary W1/W2
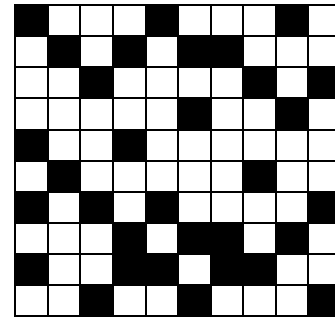
3-Intermediate z values between the boundaries W1/W2 and W2/W3 (no percolation for white zones)

4- Pseudo-phase W3

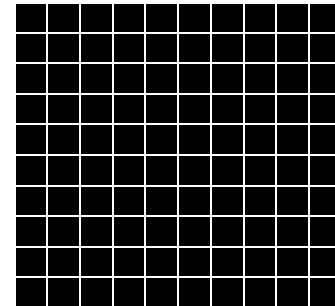**5- Limit of existence of W3 (/Fe3O4)**

Fig. 20. Three configurations for CLZ (in black) disordered distributions, typically at 1000 °C from Fe/W1 to W3/Fe$_3$O$_4$: W1 = majority of zones without defect clusters; W2 = intermediate configuration; W3 = majority of zones with defect clusters.

11. Conclusions

Point defects: Up to now, the subdivision of the equilibrium phase diagram of wüstite appears to be complex with the existence of several domains corresponding to different thermodynamic behaviors and high order transitions (at least of second order). The departure from stoichiometry can be described by a complex system of cation vacancies noted V'', V' or $V^{\mathbf{x}}$, depending on their electrical charge or neutrality, giving rise to $Fe_{Fe}^{\bullet}$ (cations Fe^{3+}) coexisting with Fe_{Fe} (cations Fe^{2+}) in octahedral sites, and $Fe_i^{\bullet\bullet\bullet}$ (cations Fe^{3+}) occupying the tetrahedral sites of the NaCl-type lattice. Changes in electrical charges must be taken into consideration, with electrons in the conduction band and holes in the valence band.

Clusters: Works from several different sources demonstrate the existence of clusters of defects constituted of iron vacancies coupled with cations Fe^{3+} in tetrahedral interstitial sites, and mixture of Fe^{2+}/Fe^{3+} cations in octahedral sites of the basic fcc lattice. These clusters can coexist with free vacancies. However, at present, the exact form of clusters noted (m:n) (m vacancies $V^{\mathbf{q}(\prime)}$ linked to n interstitials $Fe_i^{\circ\circ\circ}$) is far from being determined definitively.

33

The ratio R= $(z+t)/t$ is obtained mainly from neutron diffraction experiments in the range 2 to 4 depending on the authors. Several authors observe quasi-constant R values in the range 2 to 3, while others observe a variable or constant value in the range 2.8 to 4. It can be noted that if the wüstite lattice is occupied solely by the (m:n) isolated cluster, then the ratio R is equal to $(z+t)/t$ = m/n.

The pseudo-phases: inside the initial phase diagram, some experimental evidences from different authors support the existence of distinct areas corresponding more than likely to pseudo-phases W1, W2, W3. The term « boundary » designates a threshold of percolation at the exact separation between two thermodynamic behaviors, corresponding to progressive evolutions of short- and long-range orderings. An additional first order transition W ⇆ W' is directly linked to the first order transition α-Fe ⇆ γ-Fe at 912 °C.

Up to now, the lack of systematic studies close to the isotherm at 912 °C limits the correct definition of this part of the Fe-O phase diagram, despite the availability of some advanced thermodynamic studies. The interpretation of them remains to be developed.

Changes in cluster form: With respect to the existence of clusters (m:n) and the variation of the ratio R observed by some authors, a first description of the pseudo-phases W1, W2, W3 is proposed in terms of structure changes of these clusters, with an increasing cluster size as z increased.

The ZnS-blende type (10:4) cluster can agree with neutron diffraction experiments at equilibrium and in quenched samples, and with electron microscopy images for some compositions z of quenched samples. The (12:4) <110> specific cluster, proposed by Lebreton and Hobbs, can also agree with a superstructure of P″ type (5a x 5a x 10a) for a sufficiently high composition z.

The existence of separated ordered cluster zones can agree with the slowly variable k parameter. Let us note that significant changes in cluster form (*e.g.*, (13:4) or (10:4) transformed into (4:1)) as z or T vary have never been demonstrated for the entire phase diagram. In addition, in studies of samples at equilibrium or after a quenching process, all observations of superstructure Bragg peaks or diffuse scattering due to disorder show that the k value (k close to 2.6-2.7) varies slowly with z, thus characterizing a quasi-constant repetition distance between clusters. If the form of clusters (m:n) would change strongly, the repetition distance k.a would also change strongly, which is not observed.

New possible description of the pseudo-phases: Pseudo-phase W1 (low z values and high T values) would be characterized likely by free vacancies coexisting with a weak proportion of small zones of clusters. Pseudo-phase W3 (high z values and low T values) would correspond to clusters covering the whole lattice with a minimum distance of 2.55a between clusters and to a 5X superstructure resulting from a zigzag ordering of clusters. Pseudo-phase W2 is identified as a solution of W1 and W3 of opposite energetic evolutions above its critical temperature near 300 °C. This pseudo-phase is likely constituted of zones of ordered clusters and zones of free vacancies, with a progressive build up from boundary $z_{1/2}$ to boundary $z_{2/3}$ at which the junction arises between cluster zones that percolate.

The p to n transition might be associated with a starting of this percolation. This transition could be located in the W2 domain in a non-exclusive manner and is likely connected with a given change in electrical charges of vacancies and clusters.

Finally, an additional feature can explain the observed electrical modifications. As z increases, the electrical charges of vacancies ($V^{q(\cdot)}$= V″, V′ or V^x) and clusters could change with q varying from q=2 (low z) to q=0 (high z), due to interactions between charges. This modification of charges q is associated with an increasing number of electrons populating the conduction band.

Transition close to 912 °C: Up to now, the three varieties W'1, W'2 and W'3 associated to α-Fe below 912 °C are not strictly characterized from a structural point of view. According to Worral and Coley in their isotopic kinetic study, the defect structure identified on the surface of polycrystalline samples appears as being close to that identified for the pseudo-phases W1, W2, and W3.

Nonetheless, these authors in 2010 and 2013, following principally Wagner jr *et al.* in 1966 and Fender and Riley in 1969, have drawn new undisputable distinctions between the pseudo-phases that were identified thermodynamically as soon as 1962.

_____

Annex A

1 - Several sets from the literature of transitions located in diagram $\Theta(x)$
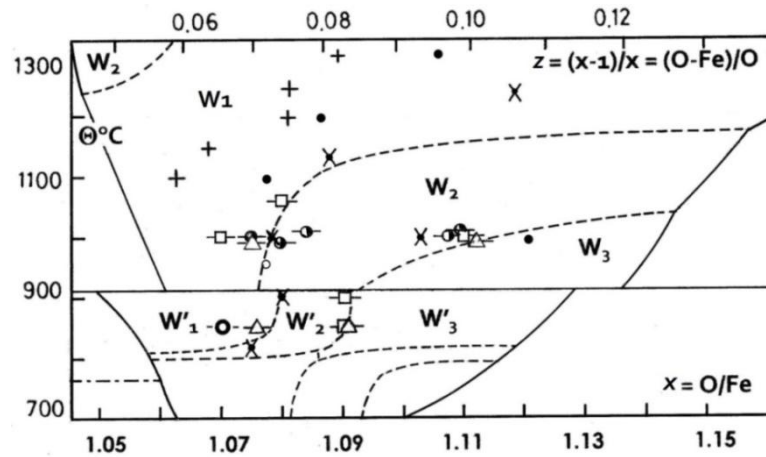
Fig. A1. Transitional effects located in the diagram [Θ °C, x].

a- Geiger, Levin, Wagner jr in ([65] p. 955 Table 4): "*unexpected changes in the slopes of log σ vs log pO$_2$*". $\Rightarrow \square$

b- Bransky, Hed [99]: breaking points at 1000, 1100, 1200, 1300 °C re-calculated for correlations of *l' vs z*. $\Rightarrow \bullet$

c- Riecke, Bohnenkamp in ([116] p.722 Fig 7): reaction rate *vs* 100*y* (Fe1-*y*O) at 1000 °C, p$_{H2O}$/p$_{H2}$) *re-analyzed* curves (I), (III) oxidation, curve (II) reduction [(I): +10°shift, (III): -10°shift]): change in slope of the quasi-linear segments. $\Rightarrow \bullet$

d- Takayama, Kimizuka in [70]; see *supra* re-analyze of the isotherms in §3.7. « *phase modifications* ». $\Rightarrow +$

e- Molenda, Stokłosa, Znamirowski in ([83] p. 517; Fig. 2 and p. 519): experimental log(σ) vs *l'* (818-1307 °C, successive segments defined from Raccah-Vallet's data to model the curvature; Fig.4: isothermal σ(y), *resulting intersections* of successive linear segments of σ(*y*) $\Rightarrow \times$

f- Worral, Coley in [73]: another interpretation of Fig. 9 at 850 °C p. 821) give rise to an additional point close to $x = 1.078$ as a second order type transition, identified for W'1 ↔ W'2. Another transition for $x = 1.090$ appears as a discontinuity at the location of the transition W'2 ↔ W'3 $\Rightarrow \triangle$

Point ω located close to $x = 1.070$ approximates the common intersection of the three lines for re-interpreting the kinetics at 850 °C (see Annex B2) $\Rightarrow \mathbf{O}$

### 2 - Two first versions of the $\Theta(x)$ phase diagram with three subdomains
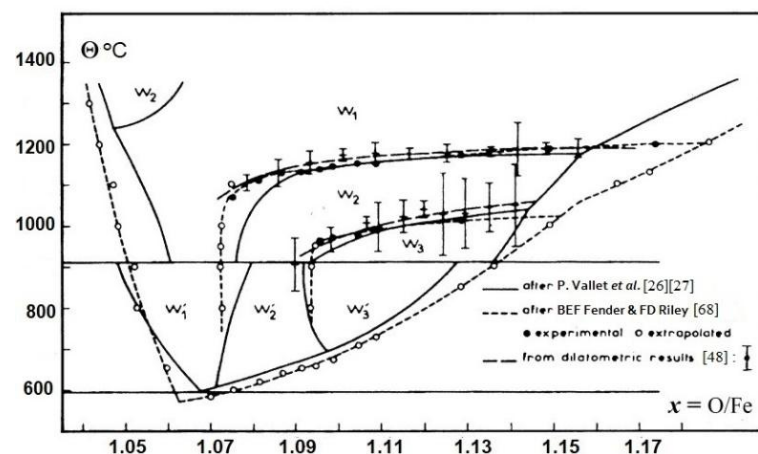
**Fig. A2. Comparative plot of experimental phase diagram versions (from ref. [50])
by Vallet and Raccah [26] and Fender and Riley [67].**

Annex B

1 - Separate diffusion sequences in the thermogravimetric study of reduction in H_2/H_2O gas mixtures

The first experimental confirmation of the three Wi out of Vallet's team is published by [65] (see *supra* in Fig. A2). At the same time, the work of Landler and Komarek [113] becomes available.
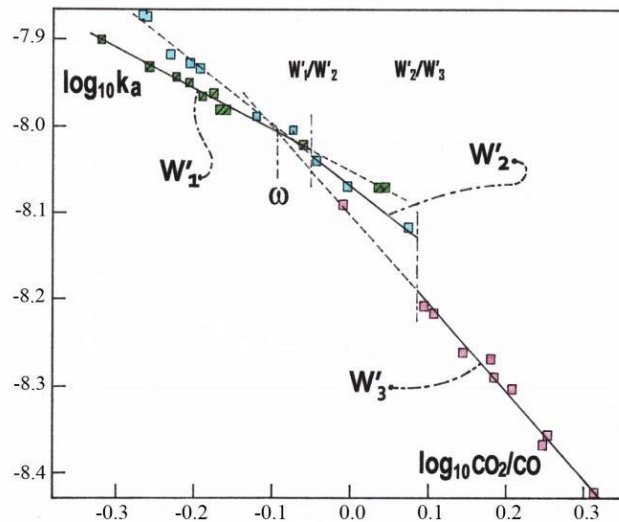
A numerical analysis makes be revealed three diffusion sequences distributed across the analyzed domain [114]. Fig. B1 is drawn as a summarized result of the determinations.
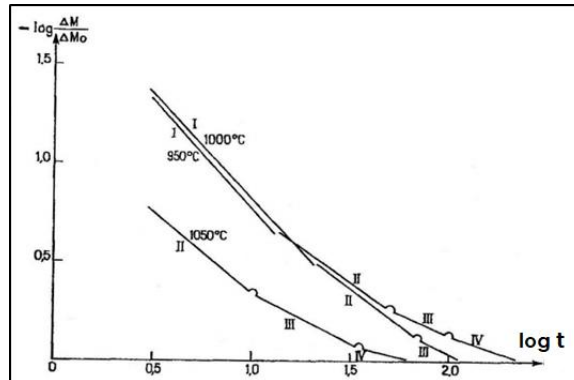
(from ref. [114])

Fig. B1. Typical runs of reduction (in H_2/H_2O gas mixtures under 1 atm) identified in ref. [113].

2 - Re-analysis of kinetic data related to the isotherm at 850 °C by Worral and Coley [73]

(identified in ref. [73])

Fig. B2. Intersection W'1/W'2 for log CO2/CO = -0.05052 => x=1.0776, expected 1.0779;
W'2/W'3 for log CO2/CO= -0.08468 => x=1.0903, expected 1.0901;
point ⍵: x = 1.0698 where the three variations are convergent.

In Fig. 9 p. 821 [73], it is possible to separate three linear variations of log k_a= -m.log (CO2/CO) + log k_0, as displayed in Fig. B2, in place of only two variations. The L.S. coefficients m = 0.48 ± 0.03 (W'1?), 0.71 ± 0.05 (W'2?), 1.03 ± 0.09 (W'3?) are statistically identical to those of equations [36], [37], [38] at 1268 K in ([73] p. 820). A discontinuity is observed at the location of the transition W'2 ↔ W'3 forecasted at equilibrium by [29]. It likely corresponds to a sharp

process in the bulk and at the surface (nuclear or electronic change in cluster structure, change in percolation mode, germination of a superstructure $(2.5a_o)$ x 3).

_____

References

[1] Goodenough JB. Metallic oxides. Pergamon Press Ltd 1971. Improved then translated into French by Casalot A: Les oxydes des métaux de transition. Collection 'Monographies de Chimie Minérale'. Paris: Gauthier-Villars; 1973. p. 166-171. French.

[2] Kofstad Per. Nonstoichiometry, diffusion, and electrical conductivity in Binary metal oxides. Wiley-Interscience; 1972. p. 221-31.

[3] Vallet P., [thermogravimetry]. Collection 'Monographies de chimie minérale'. Paris: Gauthier-Villars; 1972. [Study of the iron oxides]: p. 277-79, 294-96). French.

[4] Burgmann W. The defect structure models for wüstite: A review. Metal Science 1975; 9:169-75.

[5] Gokcen NA. Thermodynamics, Techscience Incorporated Hawthorne, California; 1975. p. 241-244.

[6] Men' AN. Bogdanovitch MP, Yu. Vorobiev YuP, Dobrovinski RYu, Kamishov VM, Fetisov VB, [Composition-defect-properties of solid phases. Method of cluster component]. Moscow « Nauka »; 1977. p. 184-90. Russian.

[7] Spencer PJ, O. Kubaschewski O. A thermodynamic assessment of the iron-oxygen system. CALPHAD 1978;2(2):147-167   https://www.sciencedirect.com/science/article/abs/pii/036459167890032-9

[8] Bauer E, Pianelli A. I: [A review of the lacunar structure of wüstite, and the necessity of new experimental researches]. Mat. Res. Bull. 1980;15(2):177-188. French.

[9] Nonstoichiometric Oxides. Academic Press, Inc. 1981, Toft Sørensen O editor; the same author, chap.1 Thermodynamics and Defect Structure of Nonstoichiometric Oxides; section IX: Recommendations for Future Work. p.1-59; chap.2 Catlow CRA, Defect clustering in nonstoichiometric oxides. p.61-98; chap.8 Cheetham AK, Structural studies on nonstoichiometric oxides using X-ray and neutron diffraction. p.399-433.

[10] Hazen RM, Jeanloz R. Wüstite (Fe1-xO): a review of its defect structure and physical properties. Rev. geophys. and space phys. 1984; 22:37-46. https://doi.org/10.1029/RG022i001p00037

[11] Gleitzer C, Goodenough JB, Mixed-valence iron oxides in structure and bonding. 61: Springer Verlag; 1985. p. 51-4.

[12] Gokcen NA. Statistical thermodynamics of alloys. New York: Plenum Press; 1986.

[13] Lykasov AA, Carel C, Men' AN, Varshavskii MT, Mikhailov GG [Physics and chemistry properties of wüstite and its solutions] Sverdlovsk: Riso Yunts AN SSSR; 1987. Russian.

[14] Mrowec S, Podgorecka A. Defect structure and transport properties of non-stoichiometric ferrous oxide. Review, J. Mater. Sci. 1987; 22:4181-9.

[15] Long GJ, Grandjean F. Mössbauer effect, magnetic and structural studies of wüstite, Fe1-xO. Adv. Solid-State, JAI Press. 1991; 2:187-221.

[16] Sundman B. An assessment of the Fe-O system, J. of Phase Equilibria Section I: basic and applied research 1991;12(1):127-40.

[17] Wriedt HA. The Fe-O (Iron-Oxygen) system. J. Phase Equilibria Section II: phase diagram evaluations 1991;12(2):169-200.

[18] Collongues R. Nonstoichiometry in Oxides. Prog. Crystal Growth and Charact. 1992; 25:203-40. About the wüstite: 209-14.

[19] Gleitzer C. Electrical properties of anhydrous iron oxides. Key Engineering Materials 1997;125-6: 355-418. About wüstite:359-80. 114 ref.:366-7).

[20] Smyth DM. The defect chemistry of metal oxides. N. Y.: Oxford University Press; 2000.

[21] Desré P, Hodaj F. Thermodynamique des matériaux. EDP Sciences; 2010. p. 76-83, 91-6, 258-66. French.

[22] Worral E, Coley KS. Defect structure of pseudo-phases of wüstite. Can. Metall. Quarterly 2013;52(1): 23-33. https://doi.org/10.1179/1879139512Y.0000000047

[23] Kröger FA, Vink HJ. Solid State Physics. Eds F. Seitz and D. Turnbull, New York: Academic Press Inc. (1956); "structure elements" 3.

[24] Schrettle F, Kant Ch, Lunkenheimer P, Mayr F, Deisenhofer J, Loidl A. Wüstite: electric, thermodynamic and optical properties of FeO. Eur. Phys. J. B 2012; 85(5) art.164, preprint (arXiv: 1203.1201) [PDF] psu.edu, [PDF] researchgate.net.

[25] Chaudron G, [Reversible reaction study of hydrogen and carbon oxide on metallic oxides] Philosophical Dissertation, Paris (1921). French.

[26] Vallet P, Raccah P, [On the boundaries of the solid wüstite domain. General diagram]. Paris: Gauthier-Villars/editions Elsevier．Compt. Rend. Acad. Sci. Paris. 1964; 258:3679-82. French. http://gallica.bnf.fr/ark:/12148/bpt6k4011c.image.r=comptes+rendus+academie+sciences+paris+1963.f1301.langFR.pagination

[27] Vallet P, Carel C. [Contribution to the study of the solid nonstoichiometric iron monoxyde. Diagram T-P(O2)-X]. Mat. Res. Bull. 1979;14(9):1181-94. French. https://doi.org/10.1016/0025-5408(79)90213-7

[28] Vallet P, Carel C, [Evaluation of the molar thermodynamic properties of solid wüstites from their equilibrium thermodynamic study, Part I: formulas for partial and integral molar properties of the three Wi and three W'i]. Rev. Chim. miné. 1986;23(3):362-77. French. ISSN: 0035- 1032/86/03 362 16; OCLC: 1871287. [Part II: boundaries of Wi and W'i stability sub-domains. Limit conditions of the integrations. Numerical assessments]. *Ibidem* 1986; 23(6):709-34. French. ISSN: 0035-1032/86/6 709 26; OCLC: 1871287.

[29] Vallet P, Carel C. The Fe-O phase diagram in the range of the nonstoichiometric monoxide and magnetite at the Fe-rich limit, Bull. Alloy Phase Diagram (=> J. of Phase Equilibria) 1989;10(3):209-18. https://doi.org/10.1007/BF02877494

[30] Jette ER, Foote F. An X-ray study of the wüstite (FeO) solid solutions. J. Chem. Phys. 1933; 1:29-3.

[31] Darken LS, Gurry RW. The System Iron-Oxygen. Part I. The Wüstite field and related equilibria. J. Am. Chem. Soc. 1945; 67:1398-412. Part II. Equilibrium and thermodynamics of liquid oxide and other phases. *ibidem* 1946; 68:788-816.

[32] Todd SS, Bonnickson KR. Low temperature heat capacities and entropies at 298.16°K of ferrous oxide, manganous oxide and vanadium monoxide. J. Am. Chem. Soc. 1951;73(8):3894-5.

[33] Humphrey GL, King EG, Kelley KK. Some thermodynamic values for ferrous oxide. Report of Investigations 4870, U. S. Department of the Interior Bureau of Mines; 1952. p. 1-16.

[34] Brynestad J, Flood H. The redox equilibrium in wüstite and solid solutions of wüstite and magnesium oxide. Zeit. Elektrochem. 1958;62(9):953-8.

[35] Roth WL. Defects in the crystal and magnetic structures of ferrous oxide. Acta Cryst. 1960; 13:140-9.

[36] Tarte P, Preudhomme J, Jeannot F, Evrard O. [IR spectrum and presence of trivalent tetrahedral iron in the structure of iron protoxide Fe1-xO (Wüstite)]. Compt. Rend. Acad. Sci. 1969;269C:1529-31. French.

[37] Wagner C, Koch E. [Electrical conductivity of cobalt and iron oxides]. Z. Phys. Chem. equilibria, J. Am. Chem. Soc. 1945;67:1398-1412. German.

[38] Wagner Carl. Thermodynamik metallischer Mehrstoffsysteme, Leipzig: Handbuch der Metallphysik Becker and Erler Kom.-Ges; 1940 Vol 1 Part 2. Enlarged and revised translation: Thermodynamics of Alloys. Addison-Wesley INC; 1952.

[39] Smyth DM. Deviations from Stoichiometry in MnO and FeO. J. Phys. Chem. Solids 1961;19(1/2): 167-169

[40] Raccah P. [Study of the thermodynamic properties of iron protoxide]. Dissertation Série B N° d'ordre 8 N° de série 7 Université de Rennes- France; 30 juin 1962. French.

[41] Raccah P, Vallet P. [On thermodynamic properties of wüstite, a strictly regular solution of iron and oxygen]. Compt. Rend. Acad. Sci. Paris 1962; 254:1038-40. French.

[42] Raccah P, Vallet P. [New set of isotherms for the solid wüstite]. Compt. Rend. Acad. Sci. Paris 1962; 255:1919-21. French.

[43] Vallet P, Kléman M, Raccah P. About new thermodynamic properties and a new phase diagram of solid wüstite. C. Rend. Acad. Sci. Paris 1963; 256:136-138. French.

[44] Vallet P, Raccah P. [Contribution to the study of the thermodynamic properties of the solid iron protoxide]. Mem. Sci. Rev. Métall. 1965; LXII(1):1-29. French.

[45] Kléman M. [Thermodynamic properties of the solid iron protoxide. Experimental results applied to the drawing of the equilibrium diagram]. Mém. Sci. Rev. Mét. (1965; LXII(6):457-469. French.

[46] Toft Sørensen O, El Sayed Ali M. Defects on metal-deficient oxides: wüstite, Fe1-yO. The Risø National Laboratory DK 4000 Roskilde: Risø-R-505. Jan. 1985: p.1-24. ISSN 0106-2840.

[47] Rekas M, Mrowec S. On defect clustering in the wustite phase. Solid State Ionics 1987; 22:185-97.

[48] Carel C, Vallet P. [Dilatometric study of diverse varieties of solid wüstite, and existence of a metastable point between the three varieties]. C. Rend. Acad. Sci. Paris 1964; 258:3281-4. French.

[49] Carel C, Weigel D, Vallet P. [Variation of the cell parameter for three wüstite varieties]. Compt. Rend. Acad. Sci. 1965; 260:4325-28. French. http://gallica.bnf.fr/ark:/12148/bpt6k4019v/f548.image

[50] Carel C, Gavarri J-R. Introduction to description of phase diagram of solid wüstite. I: structural evidence of allotropic varieties. Mat. Res. Bull. 1976;11(6):745-56.

[51] Vallet P. I: [On the thermodynamic properties of solid wüstite below 911°C], Compt. Rend. Acad. Sci. 1975; C280:239-41. II: [On the thermodynamic properties of solid wüstite above 911°C]. *Ibidem* 1975; C281:291-4. French.

[52] Pankratz LB. Thermodynamic properties of elements and oxides. US Bureau of Mines. Bulletin 672. 1982; Fe:151-3.

[53] Desai PD. Thermodynamic properties of iron. J. Phys. Chem. Ref. Data 1986;15(3):967-83.

[54] Chase jr MW. NIST-JANAF thermochemical tables. 4th edition J. Phys. Chem. Ref. Data, Monograph 9 Part II. 1998; Fe (crystal α- δ):1221-2.

[55] Löhberg K, Stannek W. [Thermodynamic description of the wüstite phase in its existence domain]. Ber. Bunsen Ges. Phys. Chem. 1975;79(3):244-55. German.

[56] Janowski J, Mrowec S, Stokłosa A. Determination of chemical diffusion and self-diffusion. Coefficients of iron in ferrous oxide. 1st Round Table Meeting Fe-Mn-O, Cracovie Kozubnik-Poland Sept 8-9, 1980, in Bull. Acad. Pol. Sci. Série Sciences chimiques 1981 pub. 1982; XXIX:91-101.

[57] Jacobsson E, Rosén E. Thermodynamic studies of high temperature equilibriums. 25. Solid state emf studies of the systems iron-ferrous oxide, nickel-nickelous oxide, and cobalt-cobaltous oxide in the temperature range 1000-1600 K. Scand. J. Met. 1981; 10:39-43.

[58] Guillermet AF, Per Gustafson. An assessment of the thermodynamic properties and the (*p, T*) phase diagram of iron. High Temp.-High Press. 1985; 16:591-610.

[59] Sjödén O, Seetharaman S, Staffansson L-I. On the Gibbs energy of formation of wustite, Metall. Trans. B (1986;17B:179-84.

[60] Grønvold F, Stølen S, Tolmach P, Westrum jr EF. Heat capacities of the wüstites $Fe_{0.9379}O$ and $Fe_{0.9254}O$ at temperatures 5 to 350K. Thermodynamics of the reaction $xFe(s) + (1/4) Fe_3O_4(s) = Fe_{0.7500+x}O(s) = Fe_{1-y}O(s)$ at T≈850 K, properties of $Fe_{1-y}O(s)$ to T=1000 K. Thermodynamics of formation of wüstite. J. Chem. Thermodynamics 1993; 25:1089-117.

[61] Swisher HH, Turkdogan ET. Solubility, permeability and diffusivity of oxygen in solid iron. Trans. Metall. AIME 1967; 239:426-31.

[62] Carel C, Vallet P. [About a first order transformation of magnetite at 1160 °C]. Bull. Soc. Sci Bretagne 1977-80 pub1981;52(1-4):55-59. Erratum. *Ibidem* (1982);54(1-4):113. French.

[63] Vallet P, Carel C. [Molar thermodynamic properties and transformations in nonstoichiometric magnetite in equilibrium with the wüstites]. Rev. Chim. miné. 1987;24(6):719-36. French.

[64] LiLova Ki, PearCe Ci, GorsKi C, rosso KM, navrotsKy a. Thermodynamics of the magnetite-ulvöspinel (Fe$_3$O$_4$-Fe$_2$TiO$_4$) solid solution. Amer. Mineralog. 2012; 97:1330-8.   https://doi.org/10.2138/am.2012.4076

[65] Geiger GH, Levin RL, Wagner jr JB. Studies on the defect structure of wüstite using electrical conductivity and thermoelectric measurement. J. Phys. Chem. Solids 1966;27:947-56. https://doi.org/10.1016/0022-3697(66)90066-7

[66] Swaroop B, Wagner jr JB. On the vacancy concentrations of wüstite (FeO$_x$) near the p to n transition. Trans. Metall. Soc. AIME 1967; 239:1215-8.

[67] Fender BEF, Riley FD. Thermodynamic Properties of Fe1-xO. Transitions in the Single-Phase Region. J. Phys. Chem. Solids 1969; 30:793-8. https://doi.org/10.1016/0022-3697(69)90273-X

[68] Marucco J-F, Picard C, Gerdanian P, Dode M. [Partial molar properties of oxygen mixing into the iron protoxyde at 1075°C. I.-Direct measurements of partial molar enthalpies by means of a high temperature microcalorimeter of the Tian-Calvet type]. J. Chim. Phys. 1970; 67:906-13. French. [II.-Measurements of the oxygen partial pressure in equilibrium with the protoxide. Calculation of s$_{O2}$^{M}]. *Ibidem* 914-6. French.

[69] Asao H, Ono K, Yamaguchi A, Moriyama J. Thermodynamic properties of wüstite (FeO$_{1+y}$). Memoirs Faculty Engineer. XXXII Part 1 (1970) 66-77. *Same authors*. [Defect structure]. Nippon Kinzoku Gakkaishi 1971;9: 871-7. Japanese.

[70] Takayama E, Kimizuka N. Thermodynamic properties and subphases of wustite field determined by means of thermogravimetric method in the temperature range of 1100-1300°C. J. Electrochem. Soc. 1980;127(4) 970-6. https://scholar.google.fr/scholar?hl=fr&as_sdt=0%2C5&q=Takayama+E%2C+Kimizuka+N&btn

[71] Barbero JA, Blesa MA, Maroto AJG. The lower temperature range of wustite stability field. Z. Phys. Chem. Neue Folge 1981; 124:139-47.

[72] Lykazov AA, Mikhailov GG, Chichkov VI. [Gibbs energy of formation of wüstite]. Izv. Vuzov. Tchern. Metallurgiia 1982;3:6-9. Russian.

[73] Worral EJ, Coley KS. Kinetics of the reaction of CO$_2$/CO gas mixtures with iron oxide. Metall. Materials Transactions B 2010;41B:813-23.   DOI: from   https://link.springer.com/article/10.1007/s11663-010-9358-4

[74] Herai T, Manenc J. [Study of decomposition of the iron protoxide]. Rev. Met. Mem. Sci. 1964; LXI(10):677-86. French.

[75] Manenc J. [Structure of the iron protoxyde, recent results]. Bull. Soc. Fr. minéral. Cristallogr. 1968; 91:594-9. French.

[76] Andersson B, Sletnes JO. Decomposition and ordering in Fe$_{1-x}$O. Acta Cryst. 1977; A33:268-76.

[77] Morral JE, Cahn JW. Spinodal decomposition in ternary systems. Acta Metallurgica 1971;19(10): 1037-45.

[78] Manenc J. [Existence of a superstructure in the iron protoxide]. J. Phys. Radium 1963;24(7): 447-50. French.

[79] Iijima S. High resolution EM study of wüstite Proceed. Electron. Microsc. Soc. Am. 1974; 32:352-3.

[80] Lykasov AA, Kuznetsov Yu, Pil'ko EI, Shishkov VI, Kozheurov VA. [Thermodynamics of wustite]. J. Phys. Chem. USSR 1969;43(12):1754-5. Russian

[81] Burgmann jr W, Urbain G, Frohberg MG. [Contribution to the study of the iron-sulfur system, with limitation to

the iron monosulfid (pyrrhotine)]. MEM. SCI. REV. METALL. 1968; LXV(7/8):567-78. French.

[82] Hillegas jr WJ. Ph. D. Thesis, Northwestern University 1968:Cat n°6901847; *in* Ref. [106-107].

[83] J. Molenda J, A. Stokłosa A, W. Znamirowski W, Transport properties of ferrous oxide Fe1-yO at high temperature. physica status solidi (b) 1987; 142:517- 29. *The same authors*. Electrical properties of manganese doped ferrous oxide at high temperatures. Solid State Ionics 1987; 24:39-44.

[84] Greenwood NN, Howe AT. Mössbauer studies of Fe1-xO. I.-The defect structure of quenched samples. J. Chem. Dalton Trans. 1972; 1:110-6. DOI: 10.1039/DT9720000110.

  II.-Disproportionation between 300 and 700 K. *Ibidem* 116-21. III.-Diffusion line broadening at 1074 and 1173 K. *Ibidem* 122-6.

[85] Romanov VP, Checherskaya LF. Mössbauer spectra of non-stoichiometric and stoichiometric wustites. phys. stat. sol. (b) 1972;49: K183-7.

[86] Checherskaya LF, Romanov VP, Tatsienko PA. Mössbauer effect in wustite. phys. stat. sol. (a) 1973;19(2): K177-82.

[87] Hrynkiewicz HU, Kulgawczuk DS, Mazanek ES, Pustowka AM, Tomala K, Wyderko ME. Mössbauer effect studies of ferrous oxides $Fe_{1-x}O$, phys. stat. sol. (a) 1972;9:611-6

[88] Pattek-Janczyk A, Sepiał B, Grenier J-C, Fournès L. Double electron exchange in $Fe_{1-x}O$: a Mössbauer study. Mat. Res. Bull. 1986; 21:1083-92.

[89] Tannhauser D. Conductivity in iron oxides. J. Phys. Chem. Solids 1962;23(1-2):25-34.

[90] Tchiong Tki Kong (wrongly referenced as *T. K. Hoang*), Romanov AD, Shaiovitch YaL, Zvinchuk RA. [About the structure of Fe1-*x*O]. Vestnik Leningradskogo Universiteta 1973;4(1):144-49. Russian.

[91] Shaiovitch YaL, Zvintchuk RA, Vergazov AN. Lattice of an equilibrium superstructure of wüstite $Fe_{0.90}O$. Fiz. Tverd. Tela (Leningrad) 1987; 29:1890-2, (*English translation in* Sov. Phys. Solid State 1987;29(6): 1089-90).

[92] Stroeva SS, Kul'kova NV, Temkin MI. The Isotopic Exchange between CO and CO2 on various surfaces. Proc. Acad. Sci. USSR, Physical Chemistry Section 1959;124:113-9.

[93] Temkin MI, Nakhmanovich ML, Morozov NM. Kinetics and Mechanism of Isotopic exchange and Gas Reaction on Solid Surfaces. Kinetics and Catalysis 1961;2(5):650-4.

[94] Grabke H-J. [Kinetics of oxygen exchange from CO2 to the surface of oxides]. Ber. Bunsenges. 1965;69(1):48-57. German.

[95] Cramb AW, Belton GR. Studies of the interfacial kinetics of the reaction of CO2 with liquid iron by the [14]CO2-CO isotope exchange reaction. Metall. Trans. B 1981;12B:699-704.

[96] Mori M, Morita K, Sano N. Determination of the rate of CO_2 dissociation on the surface of $CaO-SiO_2$, $CaO-Al_2O_3$, $CaO-SiO_2-CaF_2$ and $CaO-SiO_2-Fe_xO$ Melts. ISIJ International 1996;36(6):624-30.

[97] Xiaojun Hu, Teng Zhang, Hongyan Yan, Hiroyuki Matsuura, Fumitaka Tsukihashi, Kuo-Chih Chou. Interfacial rate of CO2-CO reaction with the solid iron and iron oxide by isotope exchange technique at 1 273 K. ISIJ International 2012; 52:1529-34.

[98] Teng Zhang, Xiao-jun Hu, Kuo-Chih Chou. Kinetic study on the reaction between CO2-CO and wustite using the isotope exchange method. Internat. J. of Minerals Metall. and Mater. 2013; 20:125-30.

[99] Bransky I, Hed AZ. Thermogravimetric determination of the composition-oxygen partial pressure diagram of wustite (Fe1-yO). J. Amer. Ceram. Soc.-Discussions and Notes 1968; 51:231-2.

[100] Ariya SM, Bratch BYa. Electrical conductivity of ferrous oxides at high temperatures. Fiz. Tverd. Tela 1963;5(12):3496-9. (*English translation in* Soviet Physics-Solid State, 1964(June): 2565-7)

[101] Kozheurov VA, Mikhailov GG. Electrical conductivity of wüstite. Zh. Fiz. Khim, English Translation: Russ. J. Phys. Chem. 1967;41(11):1552-5.

[102] Bransky I, Tannhauser DS. High-Temperature defect structure of ferrous oxide. Trans Metall. Soc. AIME 1967; 239:75-80.

[103] Heikes RR, Miller RC, Maradudin AA. [A study of the transport properties of semiconductors with mixed valence]. Ann. Phys. 1963;13(8):733-46. French. https://doi.org/10.1051/anphys/196313080733

[104] Lafollet P, Duquesnoy A. [On the variations of the thermoelectric power coefficient of iron protoxide as a function of the partial pressure of oxygen at high temperature]. Compt. Rend. Acad. Sci. Paris Chimie des solides 1977;284C:359-62. French.

[105] Hillegas WJ, Wagner jr JB. Effect of grain size and magnesium doping on the p to n transition in wustite. Physics Letters 1967 (20 nov.);25A(10):742-3.

[106] Gartstein E, Mason TO. Reanalysis of wüstite electrical properties. J. Amer. Ceram. Soc. 1982;65 (2):C-24-26.

[107] Hodge JD, Bowen HK. I. Measurement of low-temperature thermoelectric power for quenched wustite. J. Amer. Ceram. Soc. 1981;64(4):220-3. II. High-temperature thermoelectric power measurements in wustite. *Ibidem* 1981;64(8):431-6.

[108] Neuschütz D, Towhidi N. [Electrical conductivity of wüstite, Arch. Eisenhüttenwes]. 1970;4:303-7. German.

[109] Toroker MC, Carter AA. Hole transport in nonstoichiometric and doped wüstite. J. Phys. Chem. C 2012; 116(33):17403-13. https://pubs.acs.org/doi/10.1021/jp3047664

[110] Aldon L, Jumas J-C. Lithium-induced conversion reaction in wüstite Fe1-xO studied by [57]Fe Mössbauer. Solid State Sciences 2012; 14:354-61.

[111] Katkov AE, Lykasov AA. Wüstite solid solutions in Fe-Cu-O system. Inorganic materials 1999;35(7):706-8;

ibidem 2003;39(2):171-4.

[112] Desmarescaux P, Lacombe P. [Iron self-diffusion in the iron protoxide]. Mém. Sci. Rev. Mét. 1963; 60:899-906. French.

[113] Landler PFJ, Komarek KL. Reduction of wüstite within the wüstite phase in H2-H2O mixtures. Trans. Metall. Soc. AIME 1966; 236:138-49.

[114] Carel C. [Reduction kinetics of solid wüstite in its stability domain]. Compt. Rend. Acad. Sci. 1967; C265:533-6. French.

[115] Nowotny J, Wagner jr JB. Influence of the surface on the equilibration kinetics of non- stoichiometric oxides. Oxidation of Metals 1981;15(1/2):169-90.

[116] Riecke E, Bohnenkamp K. [About the oxidation and reduction kinetics of wüstite in its existence domain]. Archiv Eisenhüttenwesen 1969; 9:717-25. Doi.org/10.1002/srin.196904381. German.

[117] Rickert H, Weppner W. [Electrochemical investigation of the chemical diffusion in wüstite by means of an oxidizing solid electrolyte], Z. Naturforsch. 1974;29a:1849-59. German.

[118] Per Kofstad, Zeev Hed A. Defect structure model for wustite. J. Electrochem. Soc. Solid State Science 1968;115(1):102-4.

[119] Men' AN, Bogdanovitch MP, Vorobyov YP, Dobrovinski RY, Tchoufarov GI. [Thermodynamic study of nonstoichiometric solid solutions with the MO type], Comm. Coll. Internat. « Oxyde ferreux et ses solutions solides » ENSC Paris 26-28 mars 1969, Ann. Chim. 1970;5(4):309-12. French.

[120] Men' NA, Carel C. [Investigation of wüstite in its homogeneity domain by means of the Cluster Component Method]. C. R. Acad. Sc. Paris Série II Cristallochimie 1982; 253:253-6. French.

[121] Men' AN, Carel C. The cluster component method (C.C.M.) in the chemistry of non-ideal crystal structures. Application to wüstite. Solid State Chemistry: Proceed. Second Eur. Conf. Veldhoven-The Netherlands 7-9 june 1982. Elsevier: Studies in Inorganic Chemistry, Metselaar R, Heijligers HJM, Schooman J. 1983;3: 335-8.

[122] Men' AN, Carel C. The cluster component method and ordering in nonstoichiometric monoxides with the rocksalt structure. J. Phys. Chem. Sol. 1985; 46:1185-99.

[123] Catlow CRA, Fender BEF. Calculations of the defect clustering in Fe1-xO. J. Phys. C: Solid State Chem. 1975; 8:3267-79.

[124] Nowotny J, Rekas M. Defect structure and thermodynamic properties of the wustite phase (Fe1-yO). J. Amer. Ceram. Soc. 1989;72(7):1221-8.

[125] Catlow CRA, Mackrodt WC, Norgett MJ, Stoneham AM. The basic atomic processes of corrosion. II: Defect structures and cation transport in transition-metal oxides. Philosophical Magazine A 1979;40:161-72.

[126] Lebreton C, Hobbs LW. Defect structure of $Fe_{1-x}O$. Radiation Effects 1983; 74:227-36.

[127] Catlow CRA. Recent progress in defect studies of rock-salt transition metal oxides and magnetite. Metallurgia I Odlewnictwo Krakow-Poland 1987;13(1-2):31-41.

[128] Gavarri J-R, Jasienska St, Orewczyk J, Janowski J. Contribution to the study of substituted $Fe_{1-x-y}O$. Metalurgia I Odlewnictwo Krakow-Poland 1987;13(1-2):43-63.

[129] Grimes RW, Anderson AB, Heuer AH. Defect clusters in nonstoichiometric 3d transition-metal monoxides. J. Amer. Ceram. Soc. 1986; 69:619-23.

[130] Koch F, Cohen JB. The Defect Structure of Fe1-xO. Acta Cryst. 1969; B25:275-87.

[131] Gartstein E, Mason TO, Cohen JB. Defect agglomeration in wüstite at high temperatures - I: The defect arrangement. J. Phys. Chem. Solids 1986;47(8):759-73.

[132] Anderson AB, Grimes RW, Heuer AH. Defect clusters in wustite, Fe1-xO. J. Sol. State Chem. 1984; 55:353-61.

[133] Tomlinson SM, Catlow CRA. Computer simulation studies of Fe1-xO and Mn1-xO in Non-Stoichiometric Compounds Surfaces, Grain Boundaries and Structural Defects. Nowotny J, Weppner W eds. Kluwer Academic Publishers 1989;276:53-75.

[134] Minervini L, Grimes RW. Defect clustering in wüstite. J. Phys. Chem. Solids 1999; 60:235-45.

[135] Labidi M, Monty C. P' and P'' phase structures in Fe1-xO and Fe1-x-yCayO. Phase Transitions 1991; 31:99-106.

[136] Cheetham AK, Fender BEF, Taylor RI. High temperature neutron diffraction study of Fe1-xO. J. Phys. C: Solid State Chem. 1971; 4:2160-5.

[137] Battle PD, Cheetham AK. The magnetic structure of non-stoichiometric ferrous oxide. J. Phys. C : Solid State Phys. 1979;12:337-45.

[138] Saines PJ, Tucker MG, Keen DA, Cheetham AK, Goodwin AL. Coupling of the local defect and magnetic structure of wüstite Fe1-xO. Physical Review B 2013; 88:134418-8.

[139] Radler MJ, Cohen JB, Faber jr J. Point defect clusters in wüstite. J. Phys. Chem. Solids 1990;51(3):217-228.

[140] Schweika W, Hoser A, Martin M. In-situ study of the defect structure of wüstite $Fe_{1-x}O$ by diffuse elastic neutron scattering. Ber. Bunsenges. Phys. Chem. 1992;96(11):1541-4.

[141] Schweika W, Hoser A, Martin M, Carlsson AE. Defect structure of ferrous oxide $Fe_{1-x}O$. Physical Review B 1995;51(22):15771-88.

[142] Welberry TR, Christy AG. A paracrystalline description of defect distributions in wüstite, $Fe_{1-x}O$. J. Solid State Chem. 1995; 117:398-406.

[143] Welberry TR, Christy AG. Defect distribution and the diffuse X-ray pattern of wüstite, $Fe_{1-x}O$. Phys. Chem.

Minerals 1997; 24:24-38.

[144] Welberry TR, Goossens DJ, Heerdegen AP. Local order in wüstite using a pair distribution function (PDF) approach. Mineralogical Magazine 2014;78(2):373-85.

[145] Gavarri J-R, Carel C, Weigel D. [Contribution to the structural study of solid wüstite at high temperature]. J. Sol. State Chem. 1979;29:81-95. French.

[146] Carel C, Gavarri J-R. Structural evolution study of substituted wüstites $Fe_{1-z-y}(Ca,Mg)_yO$. J. Phys. Chem. Solids 1990;51(9):1131-6.

[147] Smuts J. Structure of wüstite and the variation of its X-ray diffraction intensities with composition. J. Iron Steel Inst. 1966 (Mars):237-9.

[148] Ishiguro T, Nagakura S. Structure of the commensurate phase P″of wüstite $Fe_{0.902}O$ studied by high resolution electron microscopy. Japan. J. Applied Phys. 1985;24(9): L723-6.

[149] Gavarri J-R, Carel C, Weigel D. Re-examination of the cluster structure on quenched wüstites of P′ and P″ types. C. Rend. Acad. Sci. Paris Cristallographie 1988;307(Série II):705-10 (in French + abridged English version)

[150] Nihoul G, Gavarri J-R, Carel C. The commensurate (10/4) cluster model in quenched wüstite P″. New simulation of HREM direct images. Acta Cryst. 1991; B47:333-7.

[151] Gavarri J-R, Carel C, Jasienska St, Janowski J. [Morphology and structure of wüstite. Evolution of defect clusters], Rev. Chim. miné. 1981;18:608-24. French.

[152] Bauer E, Pianelli A, Aubry A, Jeannot F. II: [New structural examination of pure and substituted metastable wüstites]. Mat. Res. Bull. 1980;15(3):323-37. French.

[153] Gartstein E, Cohen JB, Mason TO. II: An electrical conduction model. J. Phys. Chem. Solids 1986;47(8):775-81.

[154] Yamamoto A. Modulated structure of wustite (Fe1-xO) (Three-dimensional modulation). Acta Cryst. 1982; B38: 1451-6.

[155] Weigel D, Veysseyre R, Carel C. [About symbols of the space group of a tri-incommensurate cubic wüstite, and Bravais groups of its crystal family in the 6-dimensional Euclidean space]. Compt. Rend. Acad. Sci. 1987; 305(II):349-52. French.

[156] Gavarri JR, Carel C. Structure of wüstite at high temperature. Composite picture. Proceed. Round Table Meeting Iron and Manganese Oxides Sept. 8-9, 1980, Bull. Acad. Mines Metall. Akademia Gorniczo Hutnicza im. Stanisława Staszica w Krakowie 1982(R):7-20.

———————————————